Journal of Fluids and Structures (1999) **13,** 551–578
Article No.: jfls. 1999.0219, available online at http://www idealibrary com. on IDEAL

A COMPARISON OF METHODS FOR EVALUATING TIME-DEPENDENT FLUID DYNAMIC FORCES ON BODIES, USING ONLY VELOCITY FIELDS AND THEIR DERIVATIVES

F. Noca, D. Shiels and D. Jeon

Graduate Aeronautical Laboratories, California Institute of Technology
Pasadena, CA 91125, U.S.A.

(Received 16 June 1998 and in revised form 12 March 1999)

We continue with the 1997 work of Noca *et al.* and offer some additional closed-form expressions (and their derivations) for the evaluation of time-dependent forces on a body in an incompressible, viscous, and rotational flow, which require only the knowledge of the velocity field (and its derivatives) in a finite and arbitrarily chosen region enclosing the body. In particular, we offer an expression for the force which only depends on the velocity field (and its derivatives) on the *surface* of an arbitrary control volume. These expressions are particularly useful for experimental techniques like Digital Particle Image Velocimetry (DPIV) which provide time sequences of 2-D velocity fields but not pressure fields. For some common flow situations (freely moving objects, flexible bodies, flying and swimming animals, low Reynolds number flows, soap film tunnels), these techniques may be more viable than traditional methods (strain gages). The formulations can also be of some interest to the Computational Fluid Dynamics (CFD) community, especially when pressure is not evaluated explicitly, such as in vorticity-based algorithms. From a theoretical point of view, they provide an *explicit* relation between loading and flow structure. In the present work, the formulations are tested on a numerical flow simulation using a high-resolution vortex method and experimentally with DPIV on a circular cylinder flow.

1. INTRODUCTION

When a bluff body is submerged into a fluid in relative motion, it experiences a force. The existence of such a force has been demonstrated long before the emergence of the science of fluid mechanics: the force of the fluid flow onto the body can be evaluated directly from the *external* force needed to hold the body onto a given trajectory. This is an *extrinsic* measurement, which can be performed with displacement gages. For infinitesimal relative displacements, strain gages are commonly used. Gharib (1999) has recently succeeded in measuring unsteady fluid forces from time displacement data of a cylinder performing large amplitude vortex-induced oscillations under the restoring force of a spring system.

Alternatively, the force exerted by the fluid on the bluff body can be derived from the equations of fluid mechanics and evaluated using measured flow-field quantities: this is an *intrinsic* measurement, upon which the present paper is based. Intrinsic methods are made possible today in experimental work, thanks to the advent of techniques such as Digital Particle Image Velocimetry (DPIV) which allow the spatial and temporal measurement of velocity fields.

An intrinsic method surpasses an extrinsic technique by its ability to measure sectional forces (Noca *et al.* 1997), small force levels [as for low Reynolds number flows, see Noca

0889–9746/99/050551 + 28 $30.00

(1997)], and fluid forces in situations where gages are not practical (flying and swimming animals, flexible cables, offshore platforms, etc.). Mostly, an intrinsic method may yield a quantitative functional relationship between the fluid-dynamic force and the vorticity patterns in the near wake of the object, which an extrinsic measurement cannot do. For instance, it may shed some light on the direct relation between the force acting on a cylinder and the various forms of vortex patterns observed in the wake of a cylinder in forced motion (Williamson & Roshko 1988). It may also help to relate wake structure to the frequency and amplitude of a freely oscillating body in a cross flow, as exemplified in many recent studies [see, for instance, Gharib (1999) or Khalak & Williamson (1997) and the references therein].

The fundamental equation for the evaluation of forces from flow-field quantities is the momentum equation in integral form. Given an arbitrary, time-dependent control volume $V(t)$ (Figure 1) bounded externally by a surface $S(t)$ and internally by the body surface $S_b(t)$, the fluid dynamic force $\mathbf{F}$ acting on a body can be expressed as (for a fluid of unit density)

$$\begin{aligned}\mathbf{F} = & -\frac{\mathrm{d}}{\mathrm{d}t}\int_{V(t)} \mathbf{u}\,\mathrm{d}V \\ & + \oint_{S(t)} \hat{\mathbf{n}}\cdot[-p\mathbf{I} - (\mathbf{u}-\mathbf{u}_S)\mathbf{u} + \mathbf{T}]\,\mathrm{d}S \\ & - \oint_{S_b(t)} \hat{\mathbf{n}}\cdot(\mathbf{u}-\mathbf{u}_S)\mathbf{u}\,\mathrm{d}S,\end{aligned} \tag{1.1}$$

where $\hat{\mathbf{n}}$ is a unit vector (see Figure 1), $\mathbf{u}$ is the flow velocity, $\mathbf{u}_S$ is the body wall velocity, p the pressure, $\mathbf{I}$ the unit tensor, and $\mathbf{T}$ the *viscous* stress tensor for an incompressible flow:

$$\mathbf{T} = \mu(\nabla\mathbf{u} + \nabla\mathbf{u}^{\mathrm{T}}),$$

where μ is the coefficient of dynamic viscosity. The surface integral over the body is null for a no-through-flow condition. It can be evaluated explicitly from known boundary conditions in the case of fluid flow through the body surface (jet thrusters, salps, etc.). As it stands, equation (1.1) requires the knowledge of the *pressure field p*.

In Computational Fluid Dynamics (CFD), the pressure can generally be solved for as one of the primitive variables (Fletcher 1991) or, as in vortex-based methods, can be evaluated by an integration of the momentum equation over the known velocity field (Koumoutsakos & Leonard 1995).

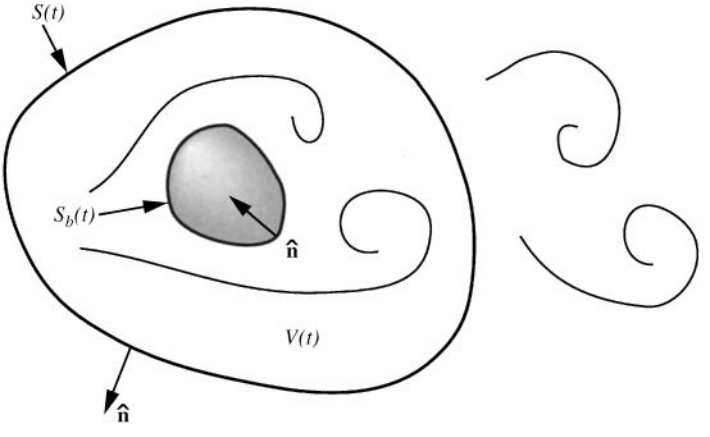

Figure 1. Domain of integration for the evaluation of fluid-dynamic forces on a bluff body.

In experimental aerodynamics, pressure and flow velocity can be measured directly, and steady-state forces can then be estimated from wake-survey methods based on equation (1.1) [for recent reviews, see Wu & Wu (1996), Brune (1994), Chometon & Laurent (1990), Maskell (1972); for classical results, see Schlichting (1986)]. Interestingly, wake-survey methods do not even require a knowledge of the pressure field for an estimation of *steady-state* lift forces [for recent work, see Wu & Wu (1996), Brune (1994), Tokumaru (1991)].

In low-speed hydrodynamics, the difficulty of performing pressure measurements may preclude the direct use of equation (1.1). Often, suitable simplifying assumptions about the pressure field can be made when wake-surveys are performed several body diameters downstream (Townsend 1976). Alternatively, when the velocity field is known, the pressure term can be obtained rigorously from an integration of the momentum equation (as in vortex-based computations). The latter method has been successfully implemented by Unal *et al.* (1998) in their PIV experiments.

However, aside from the fact that an additional step is needed to evaluate the pressure, equation (1.1) does not provide an explicit relationship between the wake configuration and the force on the body because some of the flow information is hidden in the pressure term.

With suitable algebra, some of these inconveniences can be removed by transforming equation (1.1) into a form which involves only the time derivative of the impulse over an *infinite* domain:

$$\mathbf{F} = -\frac{1}{\mathcal{N}-1}\frac{\mathrm{d}}{\mathrm{d}t}\int_{V_\infty(t)} \mathbf{x}\wedge\boldsymbol{\omega}\,\mathrm{d}V + \frac{1}{\mathcal{N}-1}\frac{\mathrm{d}}{\mathrm{d}t}\oint_{S_b(t)} \mathbf{x}\wedge(\hat{\mathbf{n}}\wedge\mathbf{u})\,\mathrm{d}S - \oint_{S_b(t)} \hat{\mathbf{n}}\cdot(\mathbf{u}-\mathbf{u}_S)\,\mathbf{u}\,\mathrm{d}S, \tag{1.2}$$

where $\boldsymbol{\omega}$ is the vorticity field, $\mathbf{x}$ the position vector, and $\mathcal{N}$ the dimension of the space ($\mathcal{N}=3$ in 3-D and $\mathcal{N}=2$ in 2-D). Note again that the integral over the body surface can be evaluated explicitly from a knowledge of the boundary conditions.

Equation (1.2) has traditionally been known to be valid for infinite fluid regions (Batchelor 1967; Lamb 1945), in which "fluidic bodies" are delineated by kinematic surfaces (Saffman 1993). Wu (1981) showed that equation (1.2) was equally valid for regions containing *solid* bodies. Lighthill (1996) did realize the importance of Equation (1.2) for the measurement of unsteady forces in field applications, such as loading on offshore structures.

Equation (1.2) requires that there be no net circulation in a 2-D space and, mostly, that the *entire* vorticity field be known. For vortex-based methods in CFD, this procedure is satisfactory since computations are carried out over a finite time during which the whole vorticity field can be accounted for (Koumoutsakos & Leonard 1995). The latter method has been applied in an experiment by Lin & Rockwell (1996) on the loading of an oscillating cylinder in quiescent water. Starting the cylinder from rest, they studied the flowfield at early times to help confine the vorticity to a small domain surrounding the body. However, in most experimental cases, it is rare for vorticity to be confined to a small domain.

Recently, Quartapelle & Napolitano (1982) succeeded in eliminating the pressure variable from equation (1.1), although at the cost of introducing an additional variable. The latter variable has the advantage of being flow-independent and only geometry-dependent, i.e., it is designed to be harmonic in the region bounded internally by the body surface and externally by the control volume boundary, with given Neumann boundary conditions on these surfaces. The resulting closed-form equation, valid for unsteady flows at arbitrary values of the Reynolds number, is based only on this geometry function and the velocity field (and its derivatives) in a finite and arbitrarily chosen region enclosing the body. For

simple body geometries (circular cylinder or sphere) and control volume boundaries at infinity, the harmonic function can be solved explicitly. Unfortunately, it needs to be solved numerically for more complicated geometries and finite control volumes. On a positive note, the asymptotic behaviour of the function at large distances from the body is such as to remove any time-derivatives from the equation when infinite domains are considered [unlike equation (1.2]). Quartapelle & Napolitano equation has recently been implemented successfully by Protas *et al.* (1999) in their numerical computations.

In the present text, we lay out alternate equations which do not exhibit the limitations of either equations (1.1) or (1.2). These are, in our terminology, the "impulse equation", the "momentum equation", and the "flux equation", which do not require the explicit evaluation of the pressure field and are based on the velocity field and its derivatives in an arbitrary, finite control volume. Besides being in closed-form, these equations are also fully explicit, unlike Quartapelle & Napolitano (1982) equation.

2. FORCE EQUATIONS

2.1 Equation I: the "Impulse Equation"

This equation was given without proof in previous work (Noca *et al.* 1997). It is an extension to equation (1.2) for a *finite* domain, and does not require the explicit evaluation of pressure.

2.1.1. *Equation I*

$$\begin{aligned}\mathbf{F} = & -\frac{1}{\mathscr{N}-1}\frac{\mathrm{d}}{\mathrm{d}t}\int_{V(t)}\mathbf{x}\wedge\boldsymbol{\omega}\,\mathrm{d}V \\ & +\oint_{S(t)}\hat{\mathbf{n}}\cdot\boldsymbol{\gamma}_{\mathrm{imp}}\,\mathrm{d}S \\ & +\frac{1}{\mathscr{N}-1}\frac{\mathrm{d}}{\mathrm{d}t}\oint_{S_b(t)}\mathbf{x}\wedge(\hat{\mathbf{n}}\wedge\mathbf{u})\,\mathrm{d}S-\oint_{S_b(t)}\hat{\mathbf{n}}\cdot(\mathbf{u}-\mathbf{u}_S)\,\mathbf{u}\,\mathrm{d}S,\end{aligned} \tag{2.1}$$

where

$$\begin{aligned}\boldsymbol{\gamma}_{\mathrm{imp}} = & \frac{1}{2}u^2\mathbf{I}-\mathbf{uu}-\frac{1}{\mathscr{N}-1}(\mathbf{u}-\mathbf{u}_S)(\mathbf{x}\wedge\boldsymbol{\omega})+\frac{1}{\mathscr{N}-1}\boldsymbol{\omega}(\mathbf{x}\wedge\mathbf{u}) \\ & +\frac{1}{\mathscr{N}-1}[\mathbf{x}\cdot(\boldsymbol{\nabla}\cdot\mathbf{T})\,\mathbf{I}-\mathbf{x}(\boldsymbol{\nabla}\cdot\mathbf{T})]+\mathbf{T}.\end{aligned}$$

2.1.2. *Proof*

The inviscid form of the "impulse equation", equation (2.1), is derived by Saffman (1993). The complete formulation for viscous and rotational flows is given by Moreau (1952). Both authors, however, use the "fluidic body" concept (Leonard 1987) to carry the algebra, and their integrations extend over the whole space including the body. Here, we present a derivation which preserves the identity of the body, i.e., integrations are carried over the fluid only.

Transformations between volume and surface integrals are performed with the configuration shown in Figure 2. Surface integrations over the umbilicus or "branch cut" S_u vanish. The volume $V(t)$ is always simply connected and is delineated externally by the surface $S(t)$ and internally by the body surface $S_b(t)$.

The space dimension $\mathscr{N}$ is kept in the formulae throughout the derivations. However, most of the equations involve the vorticity vector which can be defined rigorously only in

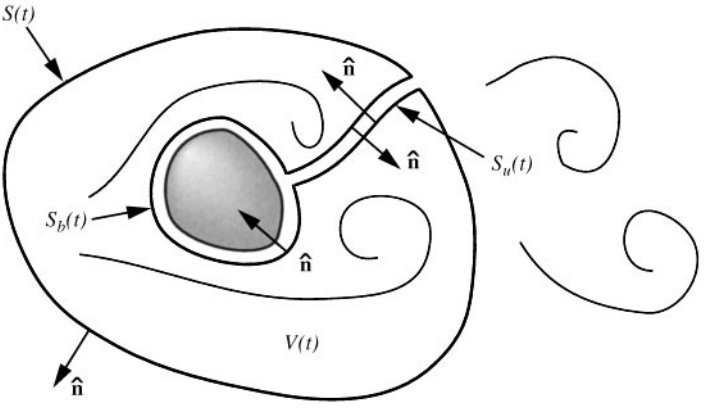

Figure 2. Control volume analysis.

three dimensions, that is $\mathcal{N} = 3$. Nevertheless, a vorticity vector for planar flows can be defined by extending the vortex lines to infinity in a direction normal to the plane of the flow. In this case, the flow is effectively two-dimensional, and we can set $\mathcal{N} = 2$.

Starting from equation (1.1) and using the identity given by equation (B.1) in the Appendix B with $\mathbf{a} = \mathbf{u}$, we obtain

$$\begin{aligned}\mathbf{F} = & -\frac{1}{\mathcal{N}-1}\frac{\mathrm{d}}{\mathrm{d}t}\int_{V(t)} \mathbf{x}\wedge\boldsymbol{\omega}\,\mathrm{d}V \\ & +\frac{1}{\mathcal{N}-1}\frac{\mathrm{d}}{\mathrm{d}t}\oint_{S(t)} \mathbf{x}\wedge(\hat{\mathbf{n}}\wedge\mathbf{u})\,\mathrm{d}S + \oint_{S(t)} \hat{\mathbf{n}}\cdot[-p\mathbf{I}-(\mathbf{u}-\mathbf{u}_S)\,\mathbf{u}+\mathbf{T}]\,\mathrm{d}S \\ & +\frac{1}{\mathcal{N}-1}\frac{\mathrm{d}}{\mathrm{d}t}\oint_{S_b(t)} \mathbf{x}\wedge(\hat{\mathbf{n}}\wedge\mathbf{u})\,\mathrm{d}S - \oint_{S_b(t)} \hat{\mathbf{n}}\cdot(\mathbf{u}-\mathbf{u}_S)\,\mathbf{u}\,\mathrm{d}S. \end{aligned} \tag{2.2}$$

The time derivative of the surface integral can be manipulated through the use of a kinematic identity given by equation (B4) in Appendix B. Writing the integrand as

$$\mathbf{x}\wedge(\hat{\mathbf{n}}\wedge\mathbf{u}) = \hat{\mathbf{n}}\cdot[(\mathbf{x}\cdot\mathbf{u})\,\mathbf{I}-\mathbf{x}\mathbf{u}],$$

identity (B4) yields

$$\begin{aligned}&\frac{\mathrm{d}}{\mathrm{d}t}\oint_{S(t)} \hat{\mathbf{n}}\cdot[(\mathbf{x}\cdot\mathbf{u})\mathbf{I}-\mathbf{x}\mathbf{u}]\,\mathrm{d}S \\ &\quad = \oint_{S(t)} \hat{\mathbf{n}}\cdot\left\{\frac{\partial}{\partial t}[(\mathbf{x}\cdot\mathbf{u})\mathbf{I}-\mathbf{x}\mathbf{u}] + \mathbf{u}_S\nabla\cdot[(\mathbf{x}\cdot\mathbf{u})\mathbf{I}-\mathbf{x}\mathbf{u}]\right\}\mathrm{d}S.\end{aligned}$$

The time derivative can be transformed back to

$$\frac{\partial}{\partial t}[(\mathbf{x}\cdot\mathbf{u})\mathbf{I}-\mathbf{x}\mathbf{u}] = \mathbf{x}\wedge\left(\hat{\mathbf{n}}\wedge\frac{\partial\mathbf{u}}{\partial t}\right),$$

where the time derivative of $\mathbf{u}$ can be obtained from the Navier–Stokes equations,

$$\frac{\partial\mathbf{u}}{\partial t} = -\nabla(p+\tfrac{1}{2}u^2) + \mathbf{u}\wedge\boldsymbol{\omega} + \nabla\cdot\mathbf{T}.$$

The divergence term can be evaluated from equation (A1) in Appendix A,

$$\nabla \cdot [(\mathbf{x} \cdot \mathbf{u})\mathbf{I} - \mathbf{x}\mathbf{u}] = -(\mathcal{N} - 1)\mathbf{u} + \mathbf{x} \wedge \boldsymbol{\omega}.$$

The result is

$$\begin{aligned} &\frac{\mathrm{d}}{\mathrm{d}t} \oint_{S(t)} \mathbf{x} \wedge (\hat{\mathbf{n}} \wedge \mathbf{u})\, \mathrm{d}S \\ &\quad = \oint_{S(t)} \mathbf{x} \wedge \{\hat{\mathbf{n}} \wedge [-\nabla(p + \tfrac{1}{2}\mathbf{u}^2) + \mathbf{u} \wedge \boldsymbol{\omega} + \nabla \cdot \mathbf{T})]\}\, \mathrm{d}S \qquad (2.3) \\ &\quad + \oint_{S(t)} \hat{\mathbf{n}} \cdot \mathbf{u}_S [-(\mathcal{N} - 1)\mathbf{u} + \mathbf{x} \wedge \boldsymbol{\omega}]\, \mathrm{d}S. \end{aligned}$$

The critical step in this derivation is the transformation of the integral involving the pressure in equation (2.3) through the use of identity (B3) of Appendix B,

$$\oint_{S(t)} \mathbf{x} \wedge \{\hat{\mathbf{n}} \wedge [-\nabla(p + \tfrac{1}{2}u^2)]\}\, \mathrm{d}S = (\mathcal{N} - 1) \oint_{S(t)} (p + \tfrac{1}{2}u^2)\hat{\mathbf{n}}\, \mathrm{d}S.$$

Insertion of these results into equation (2.2) shows that the pressure term drops out, and finally yields the desired expression for the "impulse equation", Equation I.

2.1.3. *Discussion*

If in Equation **I**, the surface $S(t)$ is taken to infinity, such that it encloses the whole vorticity field — and, in two dimensions, if there is no net circulation around the body — then the surface integral over $S(t)$ vanishes and we recover the force as the time derivative of the hydrodynamic impulse, equation (1.2).

Equation I can be put in yet another form, similar to Saffman's (1993), by converting some of the surface integral terms to a volume integral:

$$\oint_{S(t)} \hat{\mathbf{n}} \cdot (\tfrac{1}{2}u^2\mathbf{I} - \mathbf{u}\,\mathbf{u})\, \mathrm{d}S = \int_{V(t)} \mathbf{u} \wedge \boldsymbol{\omega}\, \mathrm{d}V - \oint_{S_b(t)} \hat{\mathbf{n}} \cdot (\tfrac{1}{2}u^2\mathbf{I} - \mathbf{u}\,\mathbf{u})\, \mathrm{d}S. \qquad (2.4)$$

The volume integral is essentially the Kutta–Zhukovski component of the force (Noca 1997).

2.2 Equation II: the "Momentum Equation"

We now present an equivalent expression which closely parallels equation (1.1) but does not involve the pressure term.

2.2.1. *Equation II*

$$\begin{aligned} \mathbf{F} = &-\frac{\mathrm{d}}{\mathrm{d}t} \int_{V(t)} \mathbf{u}\, \mathrm{d}V \\ &+ \oint_{S(t)} \hat{\mathbf{n}} \cdot \boldsymbol{\gamma}_{\mathrm{mom}}\, \mathrm{d}S - \oint_{S_b(t)} \hat{\mathbf{n}} \cdot (\mathbf{u} - \mathbf{u}_S)\, \mathbf{u}\, \mathrm{d}S, \qquad (2.5) \end{aligned}$$

where

$$\boldsymbol{\gamma}_{\text{mom}} = \frac{1}{2}u^2\mathbf{I} + (\mathbf{u}_S - \mathbf{u})\mathbf{u} - \frac{1}{\mathcal{N}-1}\mathbf{u}(\mathbf{x}\wedge\boldsymbol{\omega}) + \frac{1}{\mathcal{N}-1}\boldsymbol{\omega}(\mathbf{x}\wedge\mathbf{u})$$
$$-\frac{1}{\mathcal{N}-1}\left[\left(\mathbf{x}\cdot\frac{\partial\mathbf{u}}{\partial t}\right)\mathbf{I} - \mathbf{x}\frac{\partial\mathbf{u}}{\partial t}\right]$$
$$+\frac{1}{\mathcal{N}-1}[\mathbf{x}\cdot(\nabla\cdot\mathbf{T})\mathbf{I} - \mathbf{x}(\nabla\cdot\mathbf{T})] + \mathbf{T}.$$

2.2.2. *Proof*
The "momentum equation" can be obtained by inserting identity (B1) with $\mathbf{a} = \mathbf{u}$ into Equation I and using some of the results of the previous section (Noca 1997).

2.2.3. *Discussion*
The interesting feature about this equation is that it can be compared directly with the original conservation of momentum relation, equation (1.1). As a matter of fact, the troublesome pressure term can now be evaluated in closed form:

$$-\oint_{S(t)} p\hat{\mathbf{n}}\,\mathrm{d}S = \oint_{S(t)} \hat{\mathbf{n}}\cdot\boldsymbol{\gamma}_p\,\mathrm{d}S, \tag{2.6}$$

where

$$\boldsymbol{\gamma}_p = \frac{1}{2}u^2\mathbf{I} - \frac{1}{\mathcal{N}-1}\mathbf{u}(\mathbf{x}\wedge\boldsymbol{\omega}) + \frac{1}{\mathcal{N}-1}\boldsymbol{\omega}(\mathbf{x}\wedge\mathbf{u})$$
$$-\frac{1}{\mathcal{N}-1}\left[\left(\mathbf{x}\cdot\frac{\partial\mathbf{u}}{\partial t}\right)\mathbf{I} - \mathbf{x}\frac{\partial\mathbf{u}}{\partial t}\right]$$
$$+\frac{1}{\mathcal{N}-1}[\mathbf{x}\cdot(\nabla\cdot\mathbf{T})\mathbf{I} - \mathbf{x}(\nabla\cdot\mathbf{T})].$$

This relation can be rearranged into the following more elegant form:

$$\oint_{S(t)} (p + \tfrac{1}{2}u^2)\hat{\mathbf{n}}\,\mathrm{d}S = \frac{1}{\mathcal{N}-1}\oint_{S(t)} \mathbf{x}\wedge(\hat{\mathbf{n}}\wedge\mathbf{v}_p)\,\mathrm{d}S, \tag{2.7}$$

where

$$\mathbf{v}_p = \frac{\partial\mathbf{u}}{\partial t} - \mathbf{u}\wedge\boldsymbol{\omega} - \nabla\cdot\,\mathbf{T}. \tag{2.8}$$

Equation (2.7) may alternatively be obtained from identity (B3), since from the Navier–Stokes equations, we have

$$\mathbf{v}_p = -\nabla(p + \tfrac{1}{2}u^2). \tag{2.9}$$

Equation (2.6) reveals that as the surface $S(t)$ is taken to infinity (thereby enclosing the whole vorticity field), the surface integral of the pressure does not vanish because of the time-derivative terms. It is possible to show that in the 3-D case, the integral is conditionally convergent and can be expressed in terms of the time derivative of the impulse (Saffman 1993; Batchelor 1967).

2.3. Equation III: the "Flux Equation"

Both Equations I and II require the evaluation of *volume integrals* over the control volume and, in particular, over the boundary layer region next to the body. Even though the "momentum equation" is more forgiving than the "impulse equation" in this respect (the former requires the volume integral of the velocity $\mathbf{u}$ only, whereas the latter asks for the moment of vorticity $\mathbf{x} \wedge \boldsymbol{\omega}$), this task may be prohibitive since boundary layers are highly under-resolved in most experimental situations.

To eliminate this inconvenience, we derive an additional equation which involves surface integrals only, with the added constraint that the velocity field be divergence free ($\nabla \cdot \mathbf{u} = 0$).

2.3.1. *Equation III*

$$\mathbf{F} = \oint_{S(t)} \hat{\mathbf{n}} \cdot \boldsymbol{\gamma}_{\text{flux}} \, \mathrm{d}S - \oint_{S_b(t)} \hat{\mathbf{n}} \cdot (\mathbf{u} - \mathbf{u}_S)\, \mathbf{u} \, \mathrm{d}S - \frac{\mathrm{d}}{\mathrm{d}t} \oint_{S_b(t)} \hat{\mathbf{n}} \cdot (\mathbf{u}\mathbf{x}) \, \mathrm{d}S, \tag{2.10}$$

where

$$\boldsymbol{\gamma}_{\text{flux}} = \frac{1}{2} u^2 \mathbf{I} - \mathbf{u}\mathbf{u} - \frac{1}{\mathcal{N}-1} \mathbf{u}(\mathbf{x} \wedge \boldsymbol{\omega}) + \frac{1}{\mathcal{N}-1} \boldsymbol{\omega}(\mathbf{x} \wedge \mathbf{u}) - \frac{1}{\mathcal{N}-1} \left[\left(\mathbf{x} \cdot \frac{\partial \mathbf{u}}{\partial t} \right) \mathbf{I} - \mathbf{x} \frac{\partial \mathbf{u}}{\partial t} + (\mathcal{N}-1) \frac{\partial \mathbf{u}}{\partial t} \mathbf{x} \right] + \frac{1}{\mathcal{N}-1} [\mathbf{x} \cdot (\nabla \cdot \mathbf{T})\, \mathbf{I} - \mathbf{x}(\nabla \cdot \mathbf{T})] + \mathbf{T}.$$

2.3.2. *Proof*

If identity (B5) or identity (B6) are inserted into Equation I or Equation II, respectively, with $\mathbf{a}$ equal to the flow velocity $\mathbf{u}$, Equation III is recovered as long as the flow is incompressible ($\nabla \cdot \mathbf{u} = 0$).

2.3.3. *Discussion*

The "flux equation" in its time-dependent form can yield time-dependent forces from data collected on an arbitrary surface *surrounding the whole body*. In the case of wakes extending downstream from the body, one could ask whether equation (2.10) could be used to estimate time-dependent forces from a wake survey only, i.e. from data collected on a surface crossing the wake arbitrarily close to the body. The question has not been tested in this work, but it is probable that the surface integration of terms involving the product of $\mathbf{x}$ and $\partial \mathbf{u}/\partial t$ does not converge at large distances *away* from the wake.

For the time-averaged case, all three equations (I, II, and III) yield the same result,

$$\langle \mathbf{F} \rangle = \oint_S \hat{\mathbf{n}} \cdot \langle \boldsymbol{\gamma} \rangle \, \mathrm{d}S - \left\langle \oint_{S_b(t)} \hat{\mathbf{n}} \cdot (\mathbf{u} - \mathbf{u}_S)\, \mathbf{u} \, \mathrm{d}S \right\rangle, \tag{2.11}$$

where brackets indicate a time-averaging procedure and

$$\langle \boldsymbol{\gamma} \rangle = \frac{1}{2} \langle u^2 \rangle \mathbf{I} - \langle \mathbf{u}\mathbf{u} \rangle - \frac{1}{\mathcal{N}-1} \langle \mathbf{u}(\mathbf{x} \wedge \boldsymbol{\omega}) \rangle + \frac{1}{\mathcal{N}-1} \langle \boldsymbol{\omega}(\mathbf{x} \wedge \mathbf{u}) \rangle + \frac{1}{\mathcal{N}-1} [\mathbf{x} \cdot \nabla \cdot \langle \mathbf{T} \rangle)\, \mathbf{I} - \mathbf{x} \nabla \cdot \langle \mathbf{T} \rangle] + \langle \mathbf{T} \rangle. \tag{2.12}$$

In the case of wakes extending downstream from the body, equation (2.11) allows the evaluation of time-averaged forces from near-wake surveys, i.e., from data collected on a surface crossing the wake arbitrarily close to the body, without any *a priori* assumption about pressure. As for any wake-survey procedure, care has to be exercised in regards to the contribution of small terms at large distances away from the wake (Wu & Wu 1996; Maskell 1972), specifically the first two terms on the right-hand side of equation (2.12), $\frac{1}{2}\langle u^2\rangle \mathbf{I}$ and $-\langle \mathbf{uu}\rangle$.

Compared to traditional wake-survey methodologies, the present formulation provides an explicit expression for the pressure contribution to the force. The original force formulation, equation (1.1), can be recast in its time-averaged form,

$$\langle \mathbf{F}\rangle = \oint_S \hat{\mathbf{n}}\cdot[-\langle p + \tfrac{1}{2}u^2\rangle \mathbf{I} + \tfrac{1}{2}\langle u^2\rangle \mathbf{I} - \langle \mathbf{u}\,\mathbf{u}\rangle + \langle \mathbf{T}\rangle]\,\mathrm{d}S$$
$$- \left\langle \oint_{S_b(t)} \hat{\mathbf{n}}\cdot(\mathbf{u}-\mathbf{u}_S)\,\mathbf{u}\,\mathrm{d}S \right\rangle,$$

where the pressure integral can be expressed in explicit form with the help of either equation (2.7) or equations (2.11) and (2.12),

$$-\oint_S \langle p + \tfrac{1}{2}u^2\rangle \hat{\mathbf{n}}\,\mathrm{d}S = \frac{1}{\mathcal{N}-1}\oint_S \mathbf{x}\wedge(\hat{\mathbf{n}}\wedge\langle \mathbf{u}\wedge\boldsymbol{\omega} + \nabla\cdot\mathbf{T}\rangle)\,\mathrm{d}S. \tag{2.13}$$

Apart from the fact that this integral can be evaluated straightforwardly from a knowledge of the velocity field, it requires data only across the limited region of the wake where vorticity and viscous effects are present.

3. NUMERICAL APPLICATION

The computational procedure has been documented in recent work (Shiels 1998; Noca *et al.* 1997), and only the basic features are presented here. A high-resolution, two-dimensional vortex-method code (Koumoutsakos & Leonard 1995) was used for the case of a circular cylinder of diameter D placed in a free stream of velocity U and performing a transverse oscillation with velocity $U\sin[(4\pi/13)\,Ut/D]$, where t denotes time. The Reynolds number, defined as $\mathrm{Re} = UD/\nu$ with ν the kinematic viscosity, was equal to 392. Figure 3 shows the vorticity field at $Ut/D = 12$ (following an impulsive start at $t = 0$). A time step of $\mathrm{d}t = 0{\cdot}0075D/U$ was used, and spatial resolution of approximately (in a Lagrangian sense) $\mathrm{d}x \approx 0{\cdot}004D$ was maintained.

The lift coefficient on the cylinder was computed with different methods:

(i) pressure and shear stress on the body surface, equation (1.1) with $S(t)$ coinciding with the body surface $S_b(t)$ (volume integrals vanish);

(ii) "impulse equation" for an infinite domain, equation (1.2);

(iii) "impulse equation" for a finite domain, equation (2.1), with ungridded data (where the domain of integration is shown by the box, fixed in the body reference frame, surrounding the cylinder in Figure 3);

(iv) "impulse equation" for a finite domain, equation (2.1), with data placed on a grid of mesh size $\sim 0{\cdot}004$D.

Since the flow is two-dimensional, the two-dimensional form of the equations was used ($N = 2$). The results for the lift coefficient are shown in Figure 4, which is reproduced for completeness from Noca *et al.* (1997). For the ungridded data, the force is computed at every time-step with time derivatives (when necessary) being evaluated from consecutive images

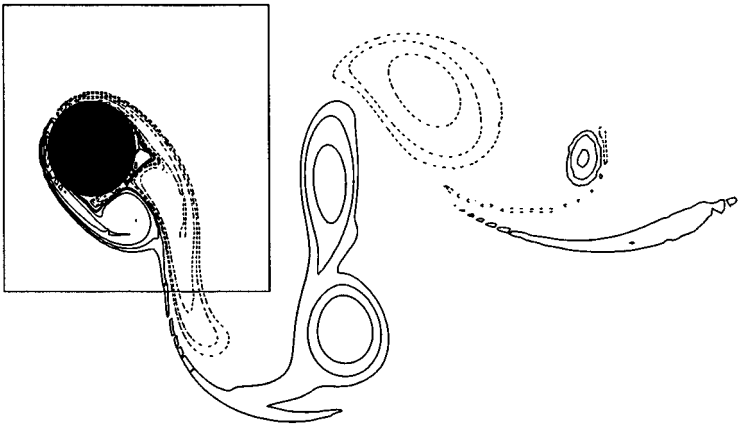

Figure 3. Vorticity field at time $Ut/D = 12$ obtained from computations, showing bounding box for force calculations (fixed in the body reference frame).

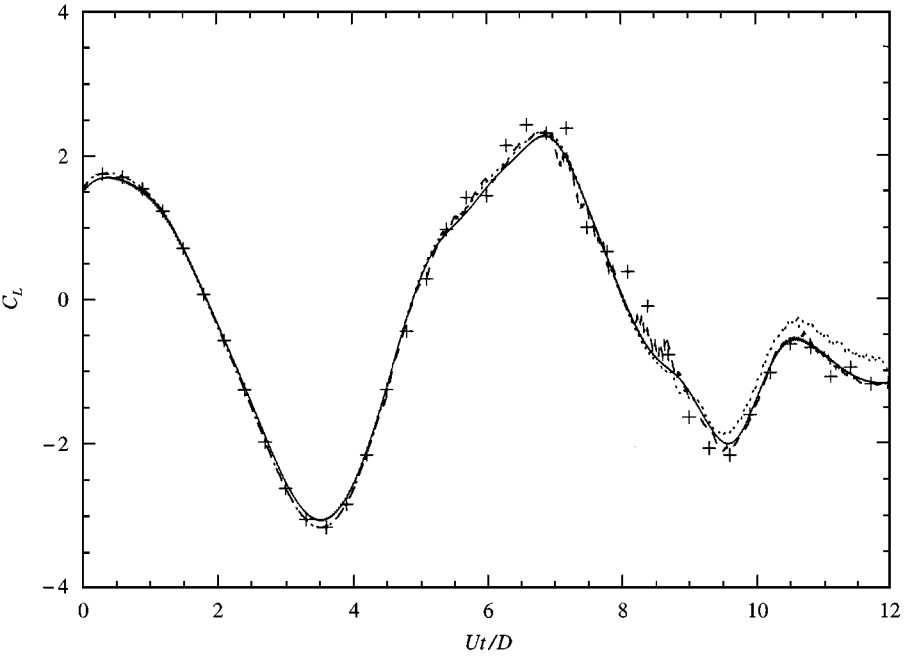

Figure 4. Comparison of lift coefficients C_L versus nondimensional time Ut/D, obtained by several methods: . . ., "impulse equation" in an infinite domain (particle-based data); ——, pressure and shear stress on the body; − − −, "impulse equation" in a finite domain (particle-based data); + + +, "impulse equation" in a finite domain (gridded data).

$0{\cdot}0075D/U$ apart, without any filtering. For the gridded data, the instantaneous forces are evaluated and plotted at instants of time $0{\cdot}3Ut/D$, using two consecutive images $0{\cdot}0075D/U$ apart for the computation of time-derivatives, without any averaging. The agreement is clearly very satisfactory.

Similar trends were obtained for the drag coefficient (Shiels 1998).

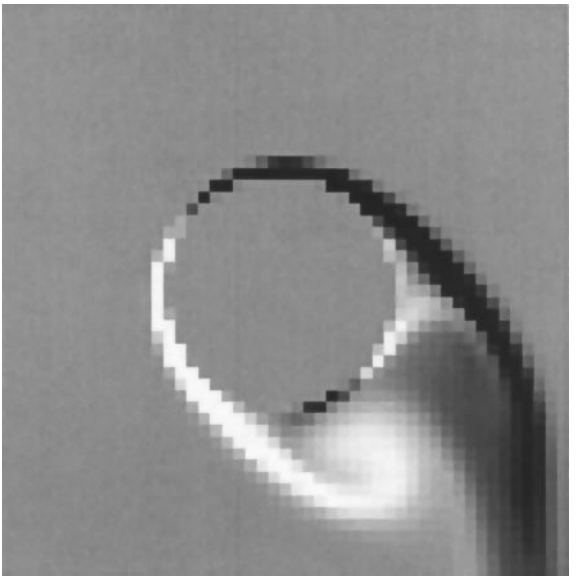

Figure 5. Vorticity field at time $Ut/D = 12$ obtained from computations, with data placed on a coarse grid.

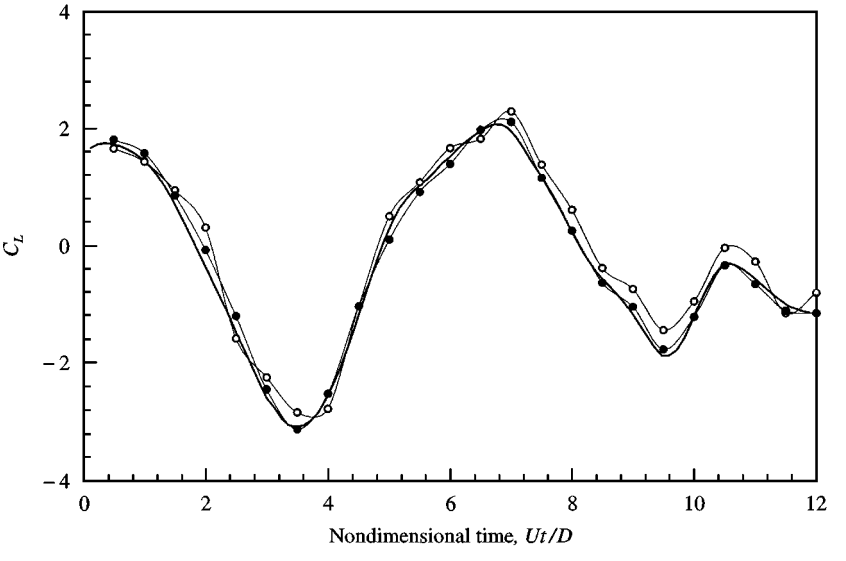

Figure 6. Comparison of lift coefficients C_L versus nondimensional time Ut/D, obtained by several methods: —, "exact" data; —○—, "impulse equation" with coarsely, gridded data; —●—, "momentum equation" with coarsely,-gridded data.

To emulate experimental situations, the (accurately resolved) numerical data was placed on a coarser grid with grid size of $\sim 0{\cdot}05D$ instead of a fine grid size of $\sim 0{\cdot}004D$ as in the previous case. A snapshot of the vorticity field placed on such a grid is shown in Figure 5 for time $Ut/D = 12$ (as in Figure 3).

The size of Figure 5 also represents the box size used for the domain of integration (it is slightly different from the one used for the well-resolved data, Figure 3). The result for the lift coefficient obtained with the "impulse equation" is shown in Figure 6 and compared to

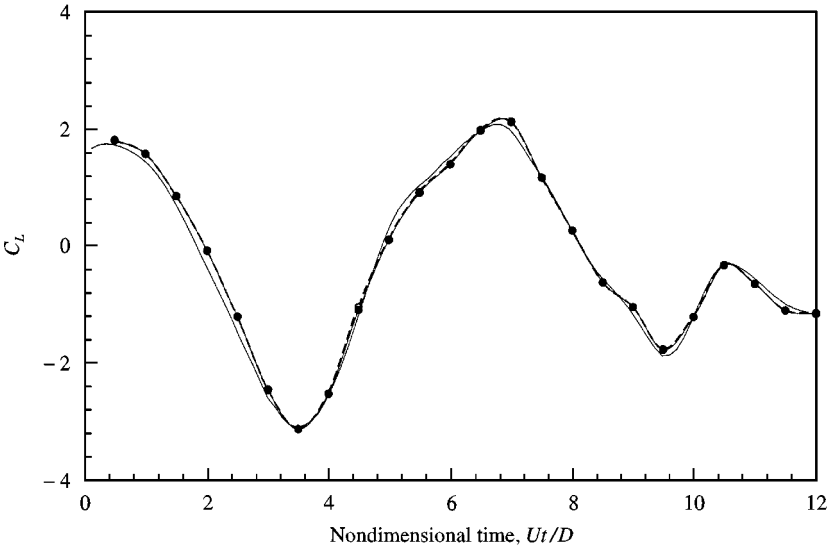

Figure 7. Comparison of lift coefficients C_L versus nondimensional time Ut/D, obtained by several methods: —, "exact" data; —○—, "momentum equation" with coarsely gridded data; —●—, "flux equation" with coarsely gridded data. (The open circle symbols may not be apparent on the graph because they lie almost exactly underneath the solid circle symbols.)

the "exact" result as obtained with the finer grid. For the coarse grid, the instantaneous forces are evaluated and plotted at instants of time $0{\cdot}5Ut/D$, using two consecutive images $0{\cdot}0075D/U$ apart for the computation of time derivatives, without any averaging.

Again, the results are very satisfactory. As a comparison, the "momentum equation" was tested on this coarsely gridded data, and Figure 6 certainly shows that the latter equation fares better than the corresponding "impulse equation". This suggests that volume integration of velocity data is preferable to volume integration of vorticity data (or more exactly, moment of vorticity data $\mathbf{x} \wedge \boldsymbol{\omega}$). We will return to this point when discussing our experimental results. The results for the "flux equation" are given in Figure 7, and again reveal a good agreement with the "exact data". As a comparison, the results using the "momentum equation" are plotted as well, and these show remarkable agreement with the "flux equation". The reason for this behaviour will be given later when comparing the "flux equation" and the "momentum equation".

4. EXPERIMENTAL APPLICATION

4.1 Experimental Setup

The experiments were conducted in the GALCIT Towing Tank (Williamson 1988). The tank is 450 cm long, 96 cm wide and 78 cm deep. The water height is typically 75 cm. On top of the tank, a carriage rides on stainless-steel wheels along two cylindrical rails which run parallel to the length of the tank. The carriage is driven by a pulley and cable system linked to a DC servo motor which is computer controlled.

The model used was a circular cylinder of diameter $D = 1$ cm. When immersed, its aspect ratio was about 75. The cylinder was held vertically and was adjusted to graze the bottom of the tank (about 2 mm off the bottom) with no end-plate at the lower end (Slaouti & Gerrard 1981).

The boundary condition at the upper end of the cylinder was dictated by the supporting mechanism for the cylinder. A 30 cm × 30 cm, $\frac{1}{2}$ in thick, Plexiglas plate was attached to

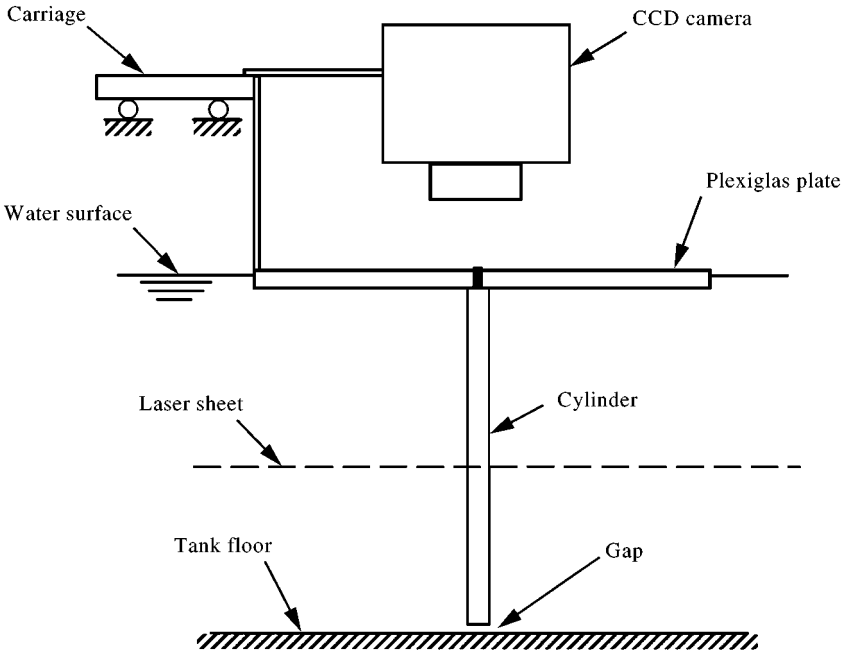

Figure 8. Sketch of experimental setup.

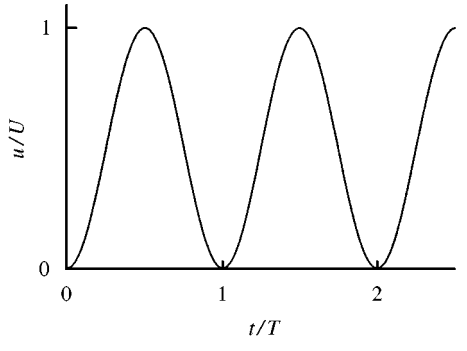

Figure 9. Carriage velocity profiles u/U versus time t/T: sinusoidal velocity profile of frequency $f = 1/T = 0{\cdot}164$ Hz with zero minimum velocity and peak velocity $U = 1$ cm/s.

the carriage and placed flat on top of the water surface. The purpose of the plate was to hold the cylinder vertically and at the same time allow optical access from the top over the whole circumference of the cylinder, as shown in Figure 8 (thereby the need for a transparent plate).

With the plexiglas plate not touching the water, a lensing effect, due to a meniscus at the cylinder and water surface junction, prevented the flowfield from being resolved very near the cylinder. We removed the problem by lowering the plexiglas plate by a couple of millimeters into the water. However, as demonstrated by Slaouti & Gerrard (1981), the plate is not an ideal boundary condition for promoting parallel shedding along the whole span of the cylinder. Nevertheless, since the motion of the cylinder was forced, the flow preserved a two-dimensional character, a necessary condition for the implementation of a force formulation with a two-dimensional technique such as DPIV.

The motion imposed on the cylinder consisted of a combined translation and in-line oscillation, as shown in Figure 9. The frequency of oscillation f was arbitrarily chosen such that it matched the natural shedding frequency of a steady cylinder flow at the peak velocity U. In nondimensional units, the essential parameters were the jerking frequency or Strouhal frequency $\mathrm{St} = fD/U = 0{\cdot}164$ and the peak Reynolds number $\mathrm{Re} = UD/\nu = 100$.

All of the results were acquired in a non-inertial frame fixed with the cylinder. In the present experiments, the forces evaluated from the flowfields were not corrected for the frame acceleration.

Velocity fields were captured with Digital Particle Image Velocimetry as described by Willert & Gharib (1991). A laser sheet was projected horizontally at the cylinder midspan, from the downstream side of the cylinder. In order to provide illumination over the whole circumference of the cylinder, including the upstream side, a thin-wall, glass cylinder filled with water was used.

The particle fields were captured with a 768×480 pixel^2 CCD camera, and later analyzed with windows of 32×32 pixel^2. During the process, the analyzing windows were overlapped such that (non-independent) velocity vectors were evaluated for every 8×8 pixel^2 region. Since the cylinder was 168 pixels in diameter on the image, the grid size for the velocity data was approximately $0{\cdot}048D$, which is similar to the coarse grid used in the computational study.

The sampling frequency for the velocity fields was 30 (in nondimensional units), which was reasonably high compared to the jerking frequency of 0·164. The flow was, thus, temporally well resolved. The spatial velocity derivatives were computed from a given velocity field image, whereas the temporal derivatives were evaluated from subsequent velocity images. Figure 10 shows an excerpt of the velocity field data collected during approximately one oscillation cycle. In actuality, about 30 images lie between one image in Figure 10 and the next. Each oscillation cycle spans approximately 180 images.

Setting the value for the Reynolds number ($\mathrm{Re} \sim 100$ to ensure two-dimensional flow) and the velocity field sampling frequency (in order for the flow to be resolved temporally) imposes a unique value on the cylinder diameter and velocity, which in turn determine the expected magnitude of forces (Noca 1997). The resulting force levels were of the order of 0.05 grams which were too low for any ordinary force balance to resolve. From a negative viewpoint, no independent force measurement could be performed, and only the self-consistency of the results could be invoked to validate the method. As a positive aspect, the present technique succeeded in measuring extremely low forces, thus circumventing the limitations of mechanical devices.

4.2. Results

4.2.1. *Temporal and spatial differentiation*

For most cases, the control volume encompassed the whole image (control volume $CV1$ in Figure 11), and the origin of the position vector was taken at the center of the cylinder at O_a. All differentiations and integrations were performed with first-order schemes on the raw velocity field data (Noca 1997). In particular, time differencing was performed on consecutive images, i.e., with a nondimensional time-step of 0·033.

A sample unfiltered data set is shown in Figure 12. The associated power spectral density of the signal is given in Figure 13. Besides the main peak at the forcing frequency of 0·164 (or $\log 0{\cdot}164 = -0{\cdot}78$ on the spectral density plot), there appears to be a peak at a frequency of approximately 10 ($\log 10 = 1$ on the spectral density plot). This high-frequency noise actually arises from the tow-tank carriage which has been documented in the past (Lisoski 1993) to vibrate at a natural frequency of approximately 10 Hz (or 10 in our nondimensional units). Because most of the signal power lies below a nondimensional

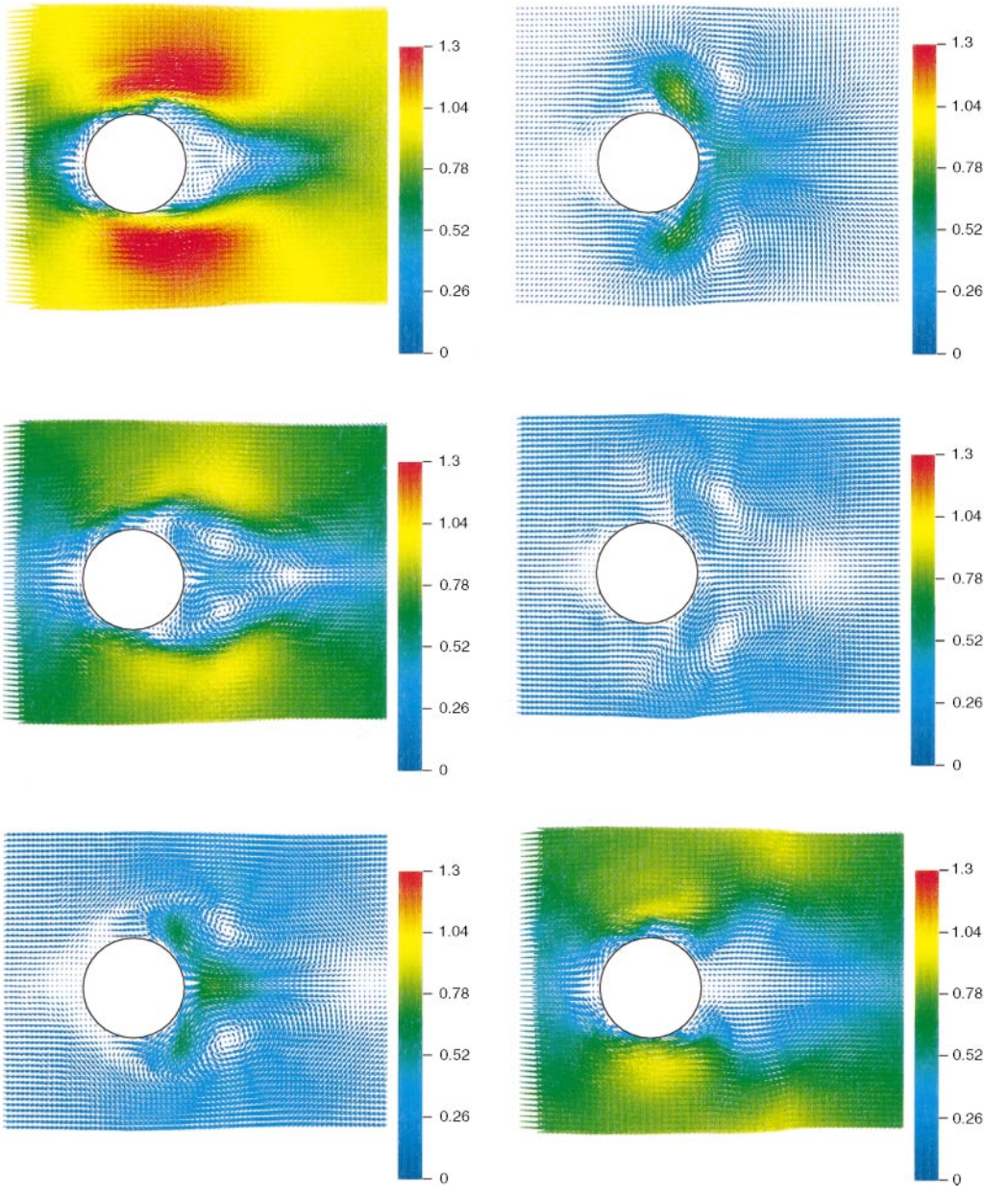

Figure 10. Experimental velocity field data obtained with DPIV for a jerking cylinder. The sequence is for one oscillation cycle starting at $Ut/D = 4$ with non-dimensional time increments of $U\delta t/D \sim 1{\cdot}02$, and runs from the top left down the column, to the top right and down the column. In the complete data, approximately 30 additional images lie between one image and the next. Color bar values indicate normalized flow velocity, u/U.

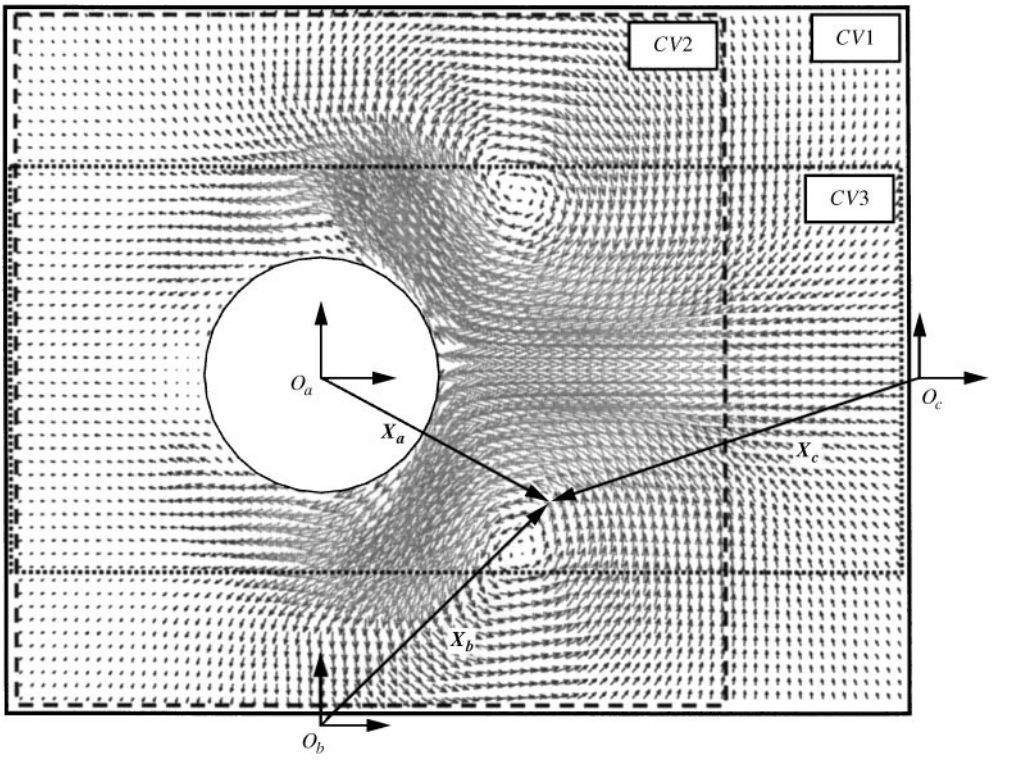

Figure 11. Sketch identifying the three control volumes $CV1$, $CV2$, and $CV3$, as well as the three co-ordinate origins O_a, O_b, and O_c, used for the parametric study. Origin O_a was used for all three control volumes, and control volume $CV1$ was used for all three origins. The boundaries are only approximate on this sketch; see text.

frequency of 1 ($\log 1 = 0$ on the spectral density plot), it was considered safe to filter the signal with a 5th order Butterworth scheme, at a low-pass cutoff frequency of 1 (well above the principal harmonic at 0·164, or $\log 0{\cdot}164 = -0{\cdot}78$ on the spectral density plot). The resulting filtered signal is shown in Figure 14.

For comparison, the force was computed also with a time-differencing step ten times larger, i.e., 0·33 instead of 0·033. The raw signal shown in Figure 15 is clearly much smoother than the one shown in Figure 12, and yet the filtered version (Figure 14) hardly differs from the signal obtained with a smaller time-differencing step.

4.2.2. *Force equations*

Forces were evaluated with the three different versions of the equations, the "impulse equation", the "momentum equation", and the "flux equation". All signals were obtained with a time-differencing step of 0·033, and filtered at a low-pass cutoff frequency of 1.

The results are shown in Figure 16 and Figure 17, and seem to be self-consistent, regardless of the equation. The "impulse equation" and the "momentum equation" seem to yield an identical answer. A slight difference ($\sim 0{\cdot}1$) is exhibited with the "flux equation".

As a repeatability test, the forces were evaluated on two distinct, but identical, runs. As shown in Figure 18, the results are satisfactorily reproducible.

4.2.3. *Geometric parameters*

The forces ought to remain unaltered with changes in the size and shape of the control volume. Figure 11 presents the three control volumes, $CV1$, $CV2$, and $CV3$, selected for the

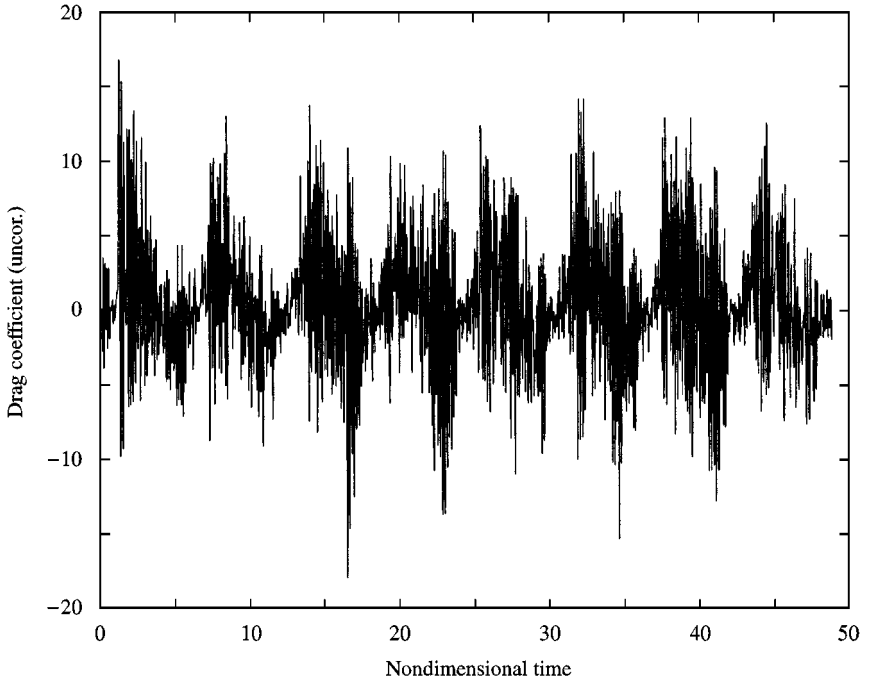

Figure 12. Unfiltered drag coefficient (uncorrected for the non-inertial, body-fixed frame) versus nondimensional time Ut/D, obtained with central time differencing (time step equal to sampling period) and the "momentum equation".

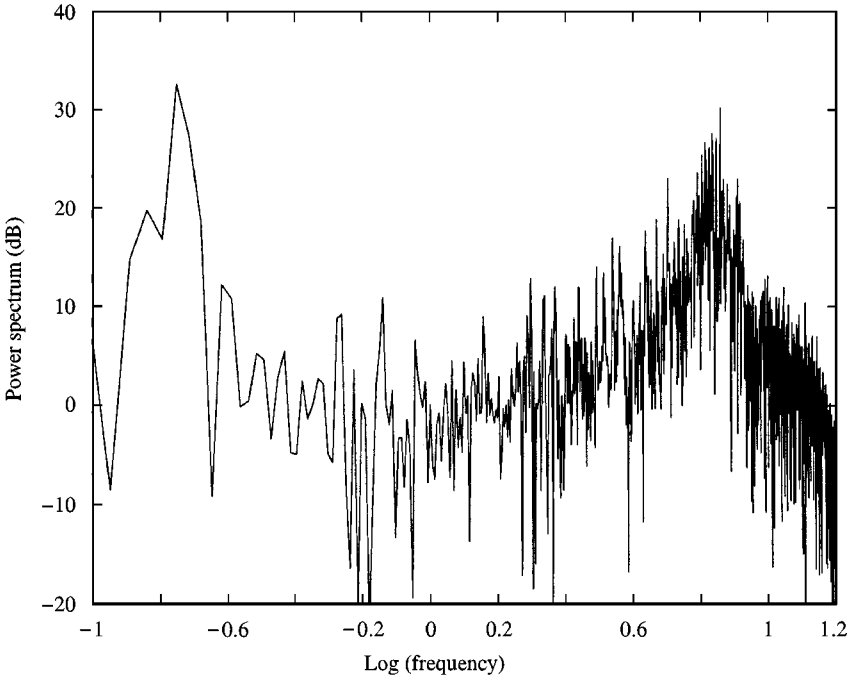

Figure 13. Power spectral density of drag coefficient, obtained with central time differencing (time-step equal to sampling period).

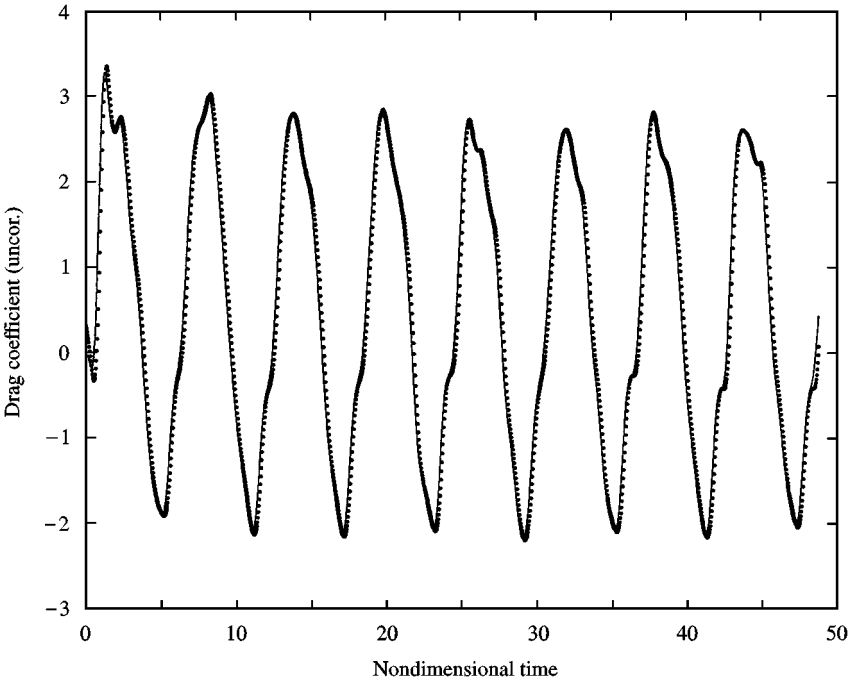

Figure 14. Drag coefficient (uncorrected for the noninertial, body-fixed frame) versus nondimensional time Ut/D, obtained with a low-pass cutoff at a frequency of 1 and the "momentum equation": ——, time-step equal to 10 times sampling period; . . . , time-step equal to sampling period.

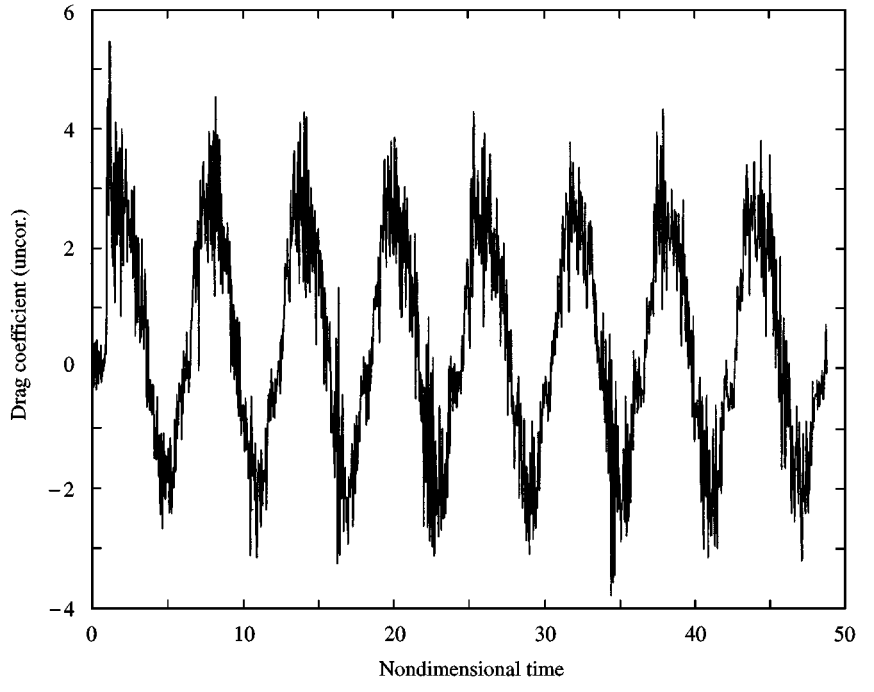

Figure 15. Unfiltered drag coefficient (uncorrected for the non-inertial, body-fixed frame) versus nondimensional time Ut/D, obtained with central time differencing (time step equal to 10 times sampling period) and the "momentum equation".

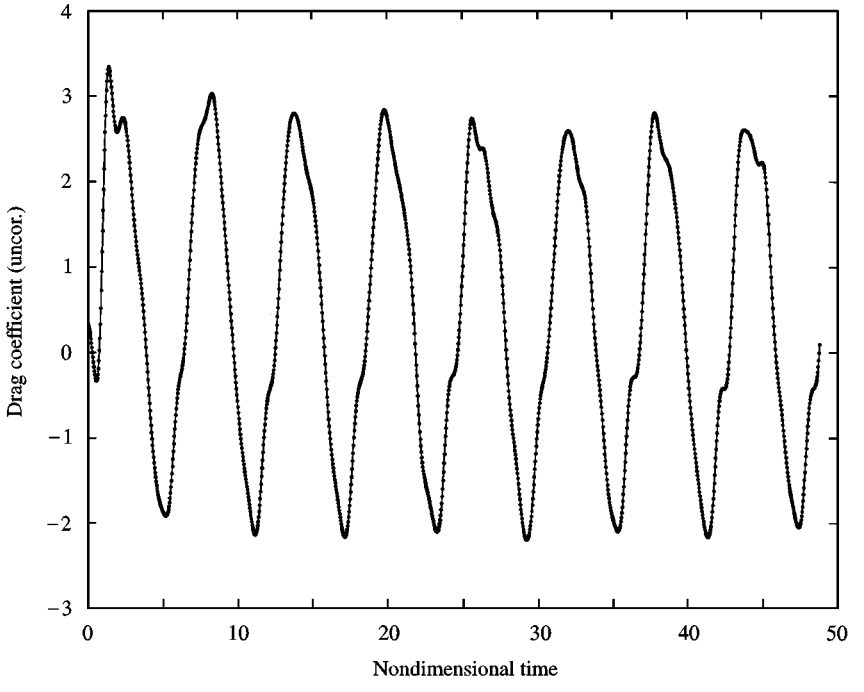

Figure 16. Drag coefficient (uncorrected for the noninertial, body-fixed frame) versus nondimensional time Ut/D, following a low-pass cutoff with a Butterworth filter at a frequency of 1: ——, "impulse equation"; . . . , "momentum equation".

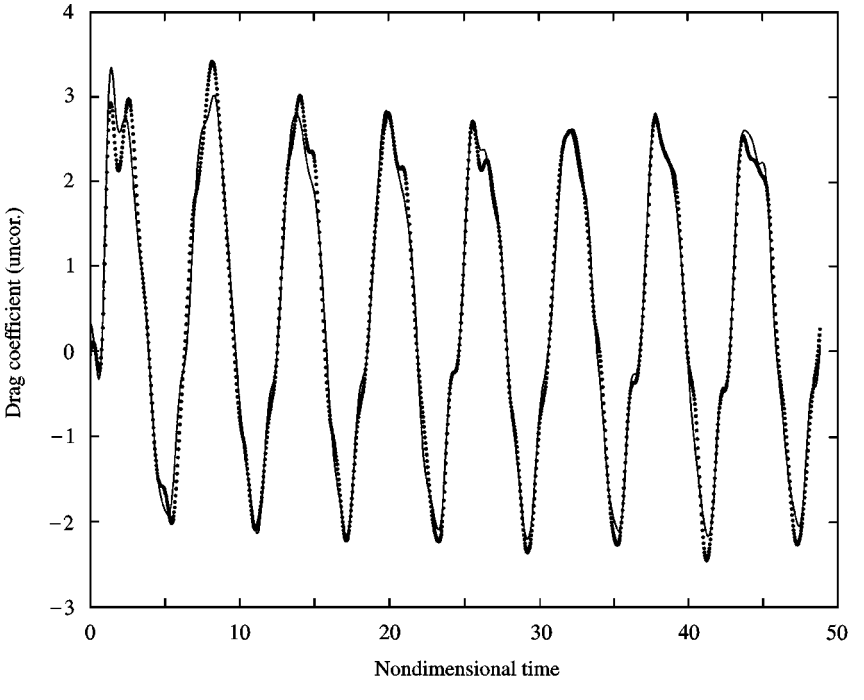

Figure 17. Drag coefficient (uncorrected for the noninertial, body-fixed frame) versus nondimensional time Ut/D, following a low-pass cutoff with a Butterworth filter at a frequency of 1: —, "momentum equation"; . . . , "flux equation".

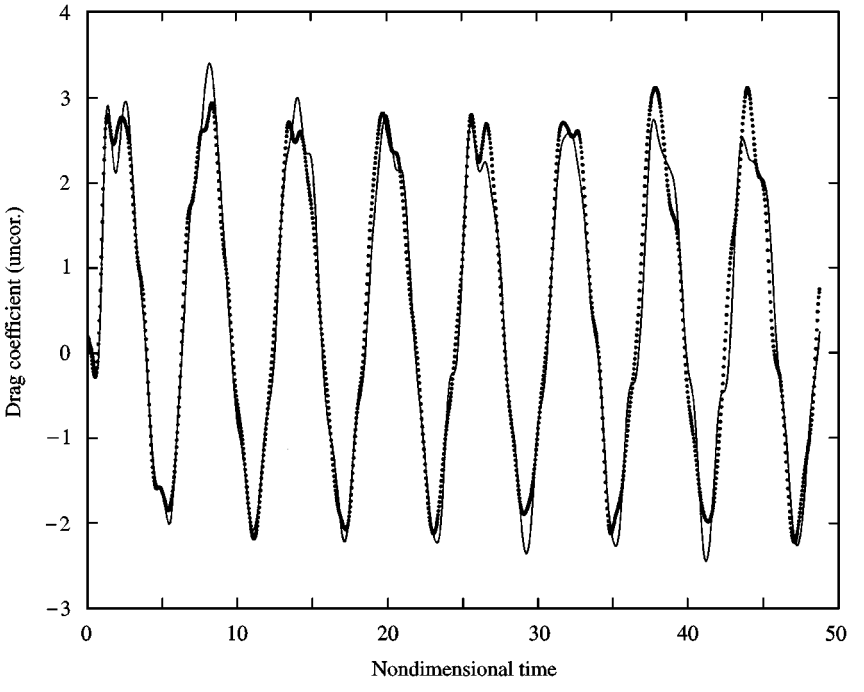

Figure 18. Drag coefficient (uncorrected for the non-inertial, body-fixed frame) versus nondimensional time Ut/D, obtained with the "flux equation" for two different runs: ——, run 1; . . . , run 2.

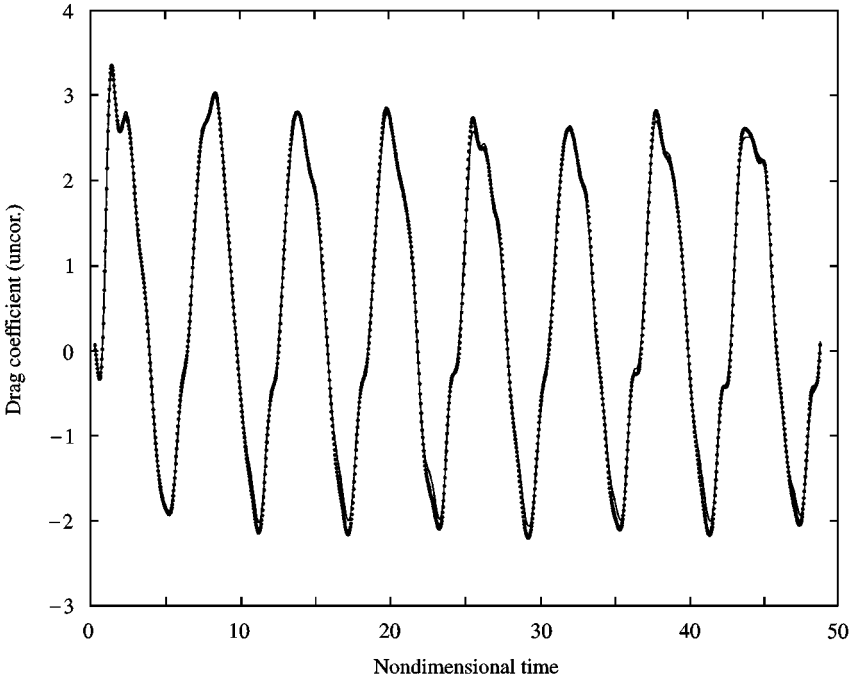

Figure 19. Drag coefficient (uncorrected for the noninertial, body-fixed frame) versus nondimensional time Ut/D, obtained with low-pass cutoff at a frequency of 1 and the "momentum equation": ——, control volume $CV2$; . . . , control volume $CV1$.

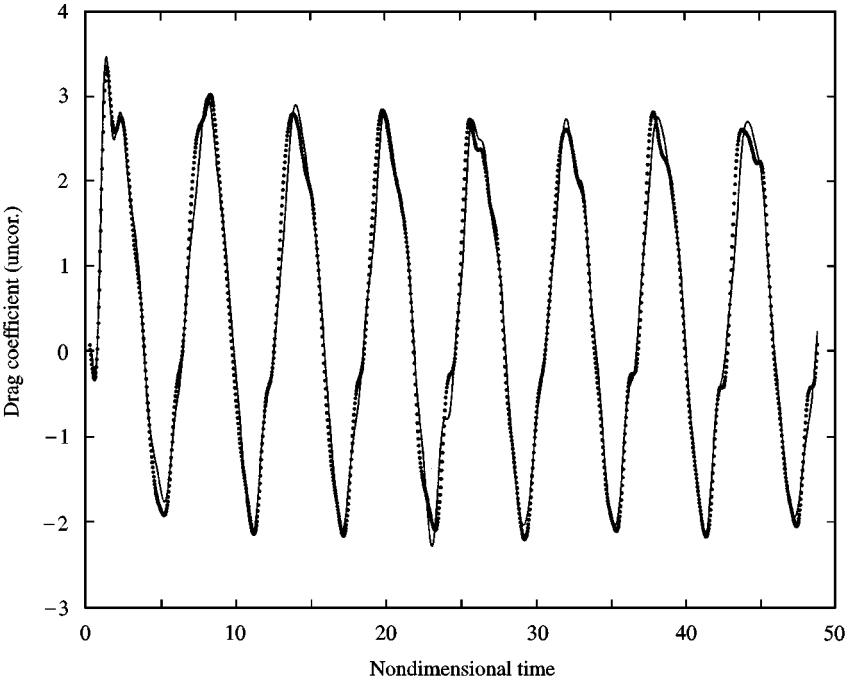

Figure 20. Drag coefficient (uncorrected for the noninertial, body-fixed frame) versus nondimensional time Ut/D, obtained with low-pass cutoff at a frequency of 1 and the "momentum equation": ——, control volume $CV3$; . . . , control volume $CV1$.

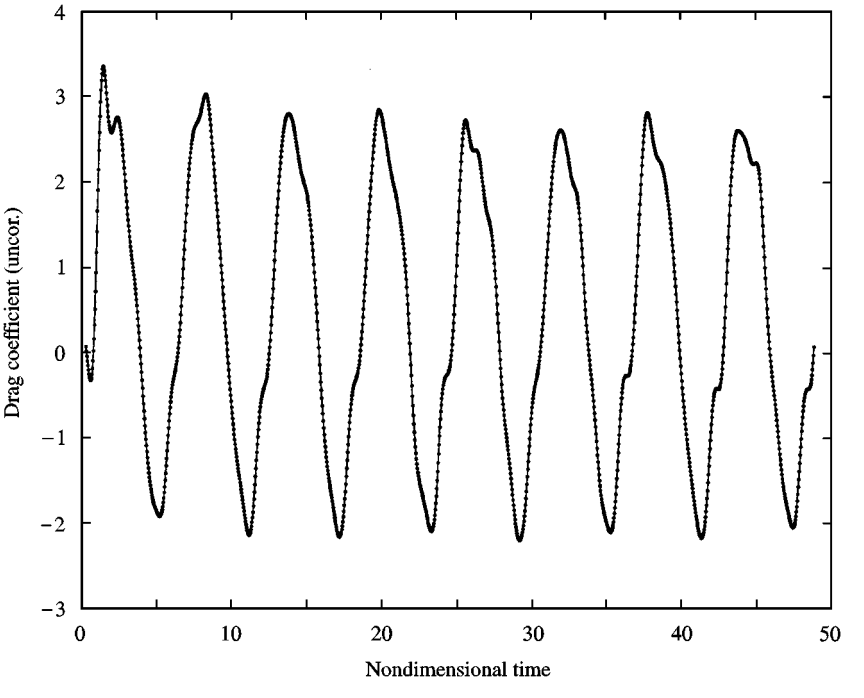

Figure 21. Drag coefficient (uncorrected for the noninertial, body-fixed frame) versus nondimensional time Ut/D, obtained with low-pass cutoff at a frequency of 1 and the "momentum equation": ——, origin O_c at the downstream edge; . . . , origin O_a at the cylinder center.

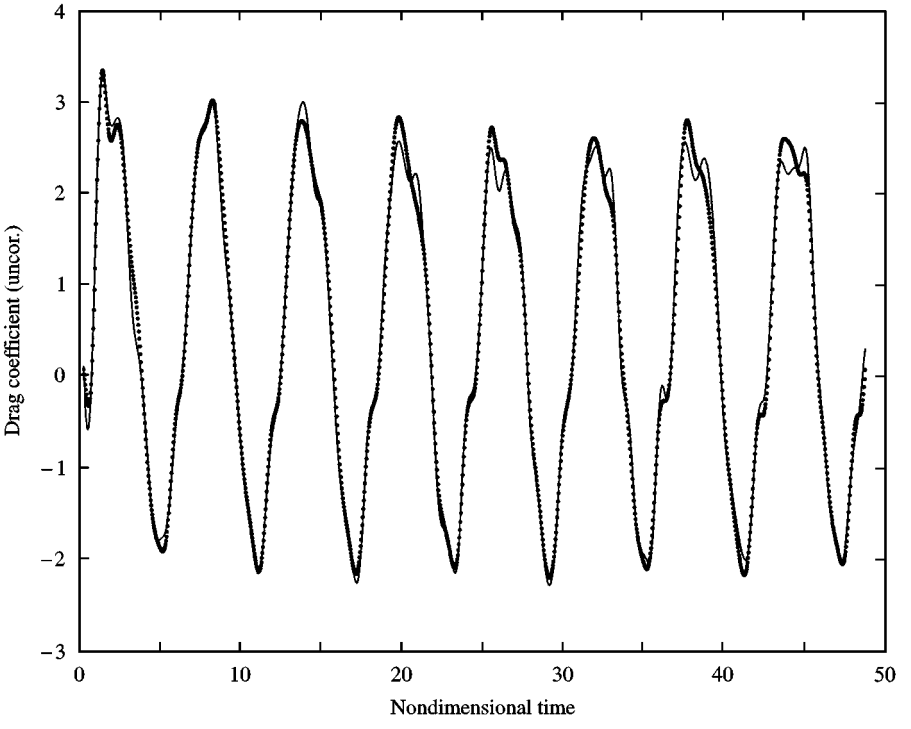

Figure 22. Drag coefficient (uncorrected for the noninertial, body-fixed frame) versus. non-dimensional time Ut/D, obtained with low-pass cutoff at a frequency of 1 and the "momentum equation": ——, origin O_b at the bottom edge; . . . , origin O_a at the cylinder center.

test, with the origin of the position vector at the center of the cylinder, O_a. With the cylinder of diameter D at coordinate (0, 0) , $CV1$ spanned $\pm 1{\cdot}4D$ in the cross-flow direction, and $(-1{\cdot}3D, +3D)$ in the flow direction; $CV2$ extended $2D$ downstream; and $CV3$ encompassed $\pm 1D$ in the cross-stream direction. Figures 19 and 20 are the result of this experiment: clearly, the signal is hardly affected by a change in control volume.

Also, since all three equations contain explicitly the position vector $\mathbf{x}$, a change of origin for this position vector is a relevant test for the self-consistency of the procedure. Control volume $CV1$ was selected for the test, and, as shown in Figure 11, O_a was chosen at the center of the cylinder, O_b at the lower edge of control volume $CV1$, and O_c at the downstream edge of control volume $CV1$. Figure 21 shows the result for the origin placed at the center of the cylinder and at the right edge of the control volume, with very good agreement. Similar consistency was obtained with the origin placed at the lower edge of the ontrol volume (Figure 22), though with lesser agreement. The reason for this behaviour can probably be attributed to the particular flow symmetry in this experiment (Figure 10). The origins O_a or O_c both lie on the line of symmetry, contrary to O_b.

5. DISCUSSION

5.1. The "Impulse Equation" and "Momentum Equation"

The "impulse equation" requires an integration of the moment of *vorticity* $\mathbf{x} \wedge \boldsymbol{\omega}$ over the volume of fluid surrounding the body. The use of such an equation may be objectionable on the grounds that the vorticity field cannot be resolved in the boundary layers next to the body. Note that only the time derivative of this integral is needed. Steady boundary layers, therefore, would not contribute to the force.

Nevertheless, the objection may be overruled by using an "improved" version of the equation, the "momentum equation", which requires only the integration of the *velocity* over the volume of fluid surrounding the body. One may argue that the *velocity* field being smoother may yield better results (Unal *et al.* 1998).

This latter statement may be correct for some experimental methodologies, but it is not in the present study. The only *measured* quantity is the velocity field. The vorticity field is a quantity *computed* from the velocity field. Since the "impulse equation" and the "momentum equation" are related by a vector identity, namely (B.2), they should theoretically yield the same answer just because they are both based on the same original data—the *velocity field*. In practice, discretization of the equations may yield a different answer. However, since the integration and differentiation schemes used in this study are linear (1st order), it is simple to show that the discretized version of identity (B.2) is satisfied identically *regardless of grid size*, which implies the equivalence of the "impulse equation" and "momentum equation" in their discretized form. This is demonstrated in Figure 16. Note that the argument holds if the flow is wholly three-dimensional because we are using the two-dimensional version of the vector identity with a vector field based on a plane. The vector field on the plane is completely arbitrary and is not even required to be divergence free.

If an experiment were set up to measure vorticity and velocity *independently*, then the two equations would probably produce different answers, depending on the accuracy of the experimental technique for measuring either fields. Higher-order discretization schemes would also yield different results for coarse grids.

The reader may be left perplexed by the numerical results shown in the previous section, which reveal a difference between the results of the "impulse equation" and "momentum equation" (Figure 6). There, the derived quantity is the velocity field which is computed from the original vorticity field (using the Biot–Savart law), based on the ungridded vortex particles. The vorticity field is only later placed on a grid (by interpolation) for the purpose of using the present equations on gridded data. Thus, it is unlikely that the velocity field and gridded vorticity field satisfy the local relation $\boldsymbol{\omega} = \nabla \wedge \mathbf{u}$ upon which vector identity (B.2) is based, and which in turn dictates the identity of the "impulse equation" and the "momentum equation". Figure 4 demonstrates the difference resulting from the use of ungridded and gridded vorticity. If the vorticity field had been re-computed from the velocity field (obtained from the Biot–Savart law) using $\boldsymbol{\omega} = \nabla \wedge \mathbf{u}$, the results from the the 'impulse equation" and the "momentum equation" would probably have been indistinguishable, regardless of grid size, for the reasons given in the previous paragraph. The accuracy of both equations remains grid-size dependent, though.

5.2 The "Momentum Equation" and "Flux Equation"

Numerically, the "momentum equation" and "flux equation" yield identical answers, as shown in Figure 7. The two equations are related by vector identity (B.6) which is identically satisfied in the computations since $\nabla \cdot \mathbf{u}$ is null by construction. In its discretized forms, vector identity (B.6) is also preserved, regardless of grid size, for the reasons discussed in the previous section regarding the "impulse equation" and "momentum equation".

The experiments exhibit a different behaviour. As just mentioned, the "flux equation" is related to the other equations through a vector identity which holds only when the velocity

field is divergence free, i.e., $\nabla \cdot \mathbf{u} = 0$, or

$$\frac{\partial u}{\partial x} + \frac{\partial v}{\partial y} + \frac{\partial w}{\partial z} = 0, \tag{5.1}$$

where u, v, and w are, respectively, the x-, y-, and z-component of the velocity field. It may be thought that this condition should be trivially satisfied if the experiments are conducted in water at low speeds, in which case the flow is practically incompressible.

However, it should be noted that the two-dimensional version of the equations is used, for which the divergence-free condition takes the form

$$\frac{\partial u}{\partial x} + \frac{\partial v}{\partial y} = 0. \tag{5.2}$$

Even though equation (5.1) is always satisfied under incompressible conditions, it is not so for equation (5.2). The solenoidal nature of the velocity field may be respected in the whole three-dimensional flow, and yet, the projection of the same velocity field onto a plane may not be divergence free.

This point is confirmed in Figure 17 where we plot the drag coefficient as obtained from the "momentum equation" and the "flux equation". There are indeed some slight differences between the two signals, and an evaluation of the velocity divergence field (Noca 1997) shows that the velocity field is non-solenoidal near the body. We do not believe that the velocity divergence arises because of actual intrinsic three-dimensionality. We think that it is an artifact of the measurement, which is quite delicate especially near the body surface. Also, since the regions near the body are regions of high strain, it may be difficult experimentally to force a large quantity such as $\partial u/\partial x$ to cancel a similarly large quantity of opposite sign $\partial v/\partial y$.

The question that arises naturally is which of the formulae, the "momentum equation" (or equivalently, the "impulse equation") or the "flux equation", gives the most reliable result (we obviously mean the *two-dimensional* versions of these equations). If the flow is actually slightly three-dimensional, we do not believe that either gives an accurate result. It is beyond the scope of the present work to include the effects of three dimensionality, but we do realize that it is a relevant consideration that ought to be studied in future work. If the flow is two-dimensional, but the measurement generates spurious divergence in the velocity field near solid boundaries, then the "flux equation" gives the most accurate answer because it does not rely on any (spurious) information contained within the control volume.

The flux equation is thus strongly preferred in situations where the flow cannot be resolved accurately near the body surface.

6. CONCLUSIONS

We have presented some exact expressions for the evaluation of body forces from velocity data. In our experiments, fluid-dynamic forces were measured by observing the flow in an arbitrary and finite domain surrounding the body. A very succinct parametric study was performed to confirm the viability of the method. It yielded satisfactory results, which can be summarized as follows.

1. The method was shown to be effective in the case of bodies in unsteady motion for which the vortex shedding pattern is very well accentuated and the normalized force coefficients are very high (~ 2–3, as for the experiments of Unal *et al.* 1998). In the process, we successfully measured time-dependent forces of the order of milligrams. Since only self-consistency was checked in these experiments, they should be repeated with a force

balance in order to produce independent measurements and thus determine the accuracy of the method.

2. The essence of the present work is the ability to perform a force analysis in a relatively small domain. We showed in particular that for large force coefficients (~ 2–3), a slight modification of the domain geometry left the results unaltered. Investigators who opt to work with larger domains or smaller force coefficients may face convergence problems while using these equations, since the formulations contain explicitly the position vector $\mathbf{x}$ which increases linearly with distance. The position vector may act as a "moment arm" which may generate large terms, which ultimately need to cancel similarly large terms in order to produce the sought force (Noca 1997). In this respect, the equation of Quartapelle & Napolitano (1982) may be more suitable because, contrary to the position vector $\mathbf{x}$, their harmonic function decays with distance. Unfortunately, the latter harmonic function is nonexplicit.

3. The effects of intrinsic three dimensionality on a nominally two-dimensional flow were not treated in this work. They are not an issue for the case of two-dimensional bodies in forced motion, for which the flow is very close to being two-dimensional. For the general case, it still remains unknown whether intrinsic three dimensionality in nominally two-dimensional flows has a direct influence on forces or whether it affects forces by modifying the large-scale (two-dimensional) structure of the flow, in which case two-dimensional PIV methods would still yield reasonable answers.

4. Noca (1997) conducted additional experiments for the case of a circular cylinder in steady motion (natural shedding) at low Reynolds number, for which the normalized lift coefficient is very low ($\sim 0{\cdot}2$). The r.m.s values for the lift coefficient compared reasonably well with those from numerical computations, and the different force equations yielded similar results. However, it was not possible to obtain self-consistent results with either a change in domain size or a relocation of the coordinates, even though the three equations compared satisfactorily for a particular choice of geometry. One reason could have been the three dimensionality of the flow induced by asymmetric end conditions and oblique vortex shedding. Another source of error mentioned above may have been "moment arm" behaviour of the position vector $\mathbf{x}$, which requires a balance between comparatively large terms to produce a small force coefficient (Noca 1997).

In conclusion, it appears that these Navier–Stokes based methods for estimating forces are very effective for flowfields that are either highly resolved or well accentuated (with large force coefficients). In particular, with present day DPIV resolution, these techniques should apply satisfactorily to bodies in forced motion (present study) or freely oscillating bodies (Gharib 1999; Khalak & Williamson 1997) for which force coefficients can be very large (~ 5). Additional work is needed to validate these methods in less favorable situations, especially for cases where force coefficients are small ($\sim 0{\cdot}2$).

ACKNOWLEDGEMENTS

We wish to acknowledge the generous support of the Office of Naval Research under grants N00014-93-1144 and N00014-94-1-0793, the Jet Propulsion Laboratory Supercomputing Project (funded from the NASA Offices of Mission to Planet Earth) for computer time, and the gracious guidance of our advisors, Professors Roshko, Leonard, and Gharib, respectively. We also would like to show our appreciation to Professor Rockwell and his group for the many useful interactions in this common effort. We are grateful to Bartosz Protas and his colleagues for informing us about their work based on the Quartapelle & Napolitano paper. We finally would like to thank our reviewers for the many useful suggestions in improving the quality of this paper.

References

Aris, R. 1962 *Vectors, Tensors, and the Basic Equations of Fluid Mechanics*. New York: Dover.

Batchelor, G. K. 1967 *An Introduction to Fluid Dynamics*. Cambridge: Cambridge University Press.

Brune, G. W. 1994 Quantitative low-speed wake surveys. *Journal of Aircraft* **31,** 249–255.

Burgatti, P. 1931 Intorno a una formula generale di trasformazione di un integrale di spazio in uno di superficie e alle sue varie deduzioni. *Bolletino della Unione Matematica Italiana* **10,** 1–5.

Chometon, F. & Laurent, J. 1990 Study of three dimensional separated flows, relation between induced drag and vortex drag. *European Journal of Mechanics* **9,** 437–455.

Fletcher, C. A. J. 1991 *Computational Techniques for Fluid Dynamics* 2nd edition. New York: Springer.

Gharib, M. 1999 Vortex-induced vibration, absence of lock-in and a novel technique for deducing the unsteady fluid force. Ph.D. thesis Graduate Aeronautical Laboratories, California Institute of Technology, Pasadena, CA 91125, U.S.A.

Khalak, A. & Williamson, C. H. K. 1997 Fluid forces and dynamics of a hydroelastic structure with very low mass and damping. *Journal of Fluids and Structures* **11,** 973–982.

Koumoutsakos, P. & Leonard, A. 1995 High-resolution simulations of the flow around an impulsively started cylinder using vortex methods. *Journal of Fluid Mechanics* **296,** 1–38.

Lamb, H. 1945 *Hydrodynamics*. New York: Dover Publications.

Leonard, A. 1987 Particle methods in fluid mechanics. *Ecole d'été d'analyse numérique*, Le Breau sans Nappe, France.

Lighthill, J. 1996 Fundamentals concerning wave loading on offshore sttructures. *Journal of Fluid Mechanics* **173,** 667–681.

Lin, J. C. & Rockwell, D. 1996 Force identification by vorticity fields: techniques based on flow imaging. *Journal of Fluids and Structures* **10,** 663–668.

Lisoski, D. L. A. 1993 Nominally 2-dimensional flow about a normal flat plate. Ph.D. thesis, Graduate Aeronautical Laboratories, California Institute of Technology, Pasadena.

Maskell, E. C. 1972 Progress towards a method for the measurement of the components of the drag of a wing of finite span. Royal Aircraft Establishment **TR 72232,** UK.

Moreau, J. J., 1952 Bilan dynamique d'un écoulement rotationnel. *Journal de Mathématiques Pures et Appliquées* **31,** 355–375; **32,** 1–78.

Noca, F. 1997 On the evaluation of time-dependent fluid-dynamic forces on bluff bodies. Ph.D. thesis, Graduate Aeronautical Laboratories, California Institute of Technology, Pasadena.

Noca, F. 1996 On the evaluation of instantaneous fluid-dynamic forces on a bluff body. GALCIT Report FM96-5.

Noca, F., Shiels, D., & Jeon, D. 1997 Measuring instantaneous fluid dynamic forces on bodies, using only velocity fields and their derivatives. *Journal of Fluids and Structures* **11,** 345–350.

Protas, B., Styczek, A. & Nowakowski, A. 1999 An effective approach to computation of forces in viscous incompressible flows. (submitted).

Quartapelle, L. & Napolitano, M. 1982 Force and moment in incompressible flows. *AIAA Journal* **21,** 911–913.

Saffman, P. G. 1993 *Vortex Dynamics*. Cambridge: Cambridge University Press.

Schlichting, H. 1987 *Boundary-Layer Theory*, 7th edition. New York: McGraw-Hill.

Shiels, D. 1998 Simulation of controlled bluff body flow with a viscous vortex method. Ph.D. thesis, Graduate Aeronautical Laboratories, California Institute of Technology, Pasadena.

Slaouti, A. & Gerrard, J. H. 1981 An experimental investigation of the end effects on the wake of a circular cylinder towed through water at low Reynolds numbers. *Journal of Fluid Mechanics* **112,** 297–314.

Thomson, J. J. 1883 *A Treatise on the Motion of Vortex Rings*. London: MacMillan & Co.

Tokumaru, P. T. 1991 Active control of the flow past a cylinder executing rotary motions. Ph.D. thesis, Graduate Aeronautical Laboratories, California Institute of Technology, Pasadena.

Townsend, A. A. 1976 *The Structure of Turbulent Shear Flow*. Cambridge: Cambridge University Press.

Truesdell, C. 1954 *Kinematics of Vorticity*. Indiana University Press.

Unal, M. F., Lin, J. C., & Rockwell, D. 1998 Force prediction by PIV imaging: a momentum-based approach. *Journal of Fluids and Structures* **11,** 965–971.

Willert, C. & Gharib, M. 1991 Digital Particle Image Velocimetry. *Experiments in Fluids* **10**, 181–193.

Williamson, C. H. K. & Govardhan, R. 1997 Dynamics and forcing of a tethered sphere in a fluid flow. *Journal of Fluids and Structures* **11,** 293–305.

Williamson, C. H. K. & Roshko, A. 1988 Vortex formation in the wake of an oscillating cylinder. *Journal of Fluids and Structures* **2,** 355–381.

WU, J. C. 1981 Theory for aerodynamic force and moment in viscous flows. *AIAA Journal* **19,** 432–441.

WU, J. Z. & WU, J. M. 1996 Vorticity dynamics on boundaries. *Advances in Applied Mechanics* **32,** 119–275.

APPENDIX A: VECTOR IDENTITIES

Most of the transformations used in this paper rely on identities which involve the position vector $\mathbf{x}$. These identities, given below, are trivial and can be proven with indicial notation:

$$\mathbf{x} \wedge (\nabla \wedge \mathbf{a}) = (\mathcal{N} - 1)\mathbf{a} + \nabla(\mathbf{x} \cdot \mathbf{a}) - \nabla \cdot (\mathbf{x}\mathbf{a}), \tag{A1}$$

$$\nabla \wedge (\mathbf{x} \wedge \phi\mathbf{I}) = -\mathbf{I}(\mathcal{N} - 1)\phi - \mathbf{I}(\mathbf{x} \cdot \nabla\phi) + \mathbf{x}\nabla\phi \tag{A2}$$

$$\nabla \cdot (\mathbf{a}\mathbf{x}) = \mathbf{x}(\nabla \cdot \mathbf{a}) + \mathbf{a}. \tag{A3}$$

In these relations, $\mathbf{a}$ is an arbitrary vector, ϕ a scalar, $\mathbf{I}$ the unit tensor, and $\mathcal{N}$ the space dimension.

APPENDIX B: INTEGRAL IDENTITIES

There are some useful integral identities, one of which is used intensively by Saffman (1993):

$$\int_V \mathbf{x} \wedge \nabla \wedge \mathbf{a}\, \mathrm{d}V = (\mathcal{N} - 1) \int_V \mathbf{a}\, \mathrm{d}V + \oint_S \mathbf{x} \wedge (\hat{\mathbf{n}} \wedge \mathbf{a})\, \mathrm{d}S, \tag{B1}$$

where $\mathbf{a}$ is an arbitrary vector field in a simply-connected volume V bounded by a surface S, $\mathcal{N}$ is the dimension of the space under consideration ($\mathcal{N} = 3$ in 3-D and $\mathcal{N} = 2$ in 2-D for example) and $\hat{\mathbf{n}}$ is the unit normal to the surface S.

Invariably, anyone trying to relate the vorticity to the velocity field will (unknowingly) "derive" this identity. As a matter of fact, setting $\mathbf{a} = \mathbf{u}$ in equation (B1) yields

$$\frac{1}{\mathcal{N} - 1} \int_V \mathbf{x} \wedge \boldsymbol{\omega}\, \mathrm{d}V = \int_V \mathbf{u}\, \mathrm{d}V + \frac{1}{\mathcal{N} - 1} \oint_S \mathbf{x} \wedge (\hat{\mathbf{n}} \wedge \mathbf{u})\, \mathrm{d}S, \tag{B2}$$

where $\mathbf{u}$ is the velocity field and $\boldsymbol{\omega} = \nabla \wedge \mathbf{u}$ the vorticity. The term on the left-hand side is the *impulse* as mentioned in the text, whereas the volume integral on the right-hand side should remind us of the flow *momentum*. It is equation (B2) (or an equation similar to it) which appears in the works of Thomson (1883), Lamb (1945), and Batchelor (1967), although it is generally obtained from integration by parts without invoking equation (B1) like it was done here. Saffman (1993) is among the few authors who calls directly upon equation (B1) for his derivations.

Burgatti (1931)—see also Truesdell (1954)—derived an identity, of which equation (B1) was a particular case. However, even though Burgatti recovered many already known fluid-dynamic identities from his generalized identity, he did not write down equation (B1) nor equation (B2) explicitly, probably because he was not aware of the latter at the time.

Thus, the identity given in equation (B1) cannot really be attributed to any single author. Also, as we shall see, its proof is quite trivial, and ought not be christened with any particular name.

The proof of this identity starts from a volume integration of the vector identity (A1):

$$\int_V \mathbf{x} \wedge (\nabla \wedge \mathbf{a})\, \mathrm{d}V = (\mathcal{N} - 1) \int_V \mathbf{a}\, \mathrm{d}V + \int_V \left[\nabla(\mathbf{x} \cdot \mathbf{a}) - \nabla \cdot (\mathbf{x}\mathbf{a})\right] \mathrm{d}V.$$

The second integral on the right-hand side can be transformed into a surface integral through Green's theorem, thus yielding

$$\int_V \mathbf{x} \wedge (\nabla \wedge \mathbf{a})\, \mathrm{d}V = (\mathcal{N} - 1) \int_V \mathbf{a}\, \mathrm{d}V + \oint_S \hat{\mathbf{n}} \cdot [(\mathbf{x} \cdot \mathbf{a})\mathbf{I} - (\mathbf{x}\mathbf{a})]\, \mathrm{d}S.$$

The surface integrand may be put into a more elegant form,

$$\begin{aligned} \hat{\mathbf{n}} \cdot [(\mathbf{x} \cdot \mathbf{a})\mathbf{I} - (\mathbf{x}\mathbf{a})] &= (\mathbf{x} \cdot \mathbf{a})\hat{\mathbf{n}} - (\hat{\mathbf{n}} \cdot \mathbf{x})\mathbf{a}, \\ &= \mathbf{x} \wedge (\hat{\mathbf{n}} \wedge \mathbf{a}) \end{aligned}$$

from which we obtain the desired result.

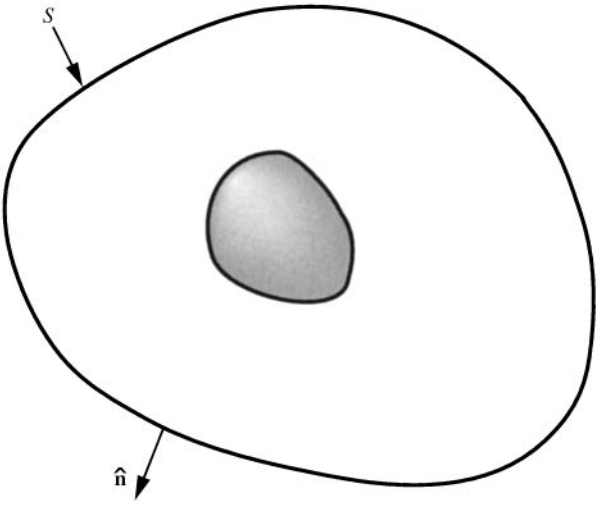

Figure 23. Doubly connected domain showing the surface of integration for the Pressure Identity.

Another useful identity, used neither by Saffman (1993) nor Moreau (1952), removes the need for integrations over the "fluidic body":

$$(\mathscr{N}-1)\oint_S \phi\hat{\mathbf{n}}\,\mathrm{d}S = -\oint_S \mathbf{x}\wedge(\hat{\mathbf{n}}\wedge\nabla\phi)\,\mathrm{d}S, \tag{B3}$$

where ϕ is a *single-valued* scalar on the surface S. Note that the domain enclosed by the surface can be *multiply connected* and need not to be simply connected (see Figure 23). This identity also appears in the paper by Wu & Wu (1996).

For a simply connected domain, identity (B3) is just a particular case of identity (B1) in which we set

$$\mathbf{a} = \nabla\phi.$$

As a matter of fact, we would have

$$\int_V \mathbf{x}\wedge\nabla\wedge(\nabla\phi)\,\mathrm{d}V = 0$$

and, from Green's theorem,

$$\int_V \nabla\phi\,\mathrm{d}V = \int_S \phi\hat{\mathbf{n}}\,\mathrm{d}S,$$

and inserting these results into identity (B1) would, in fact, yield identity (B3). The above proof is actually the one given by Saffman (1993). However, for a *multiply connected* domain, this derivation fails since the integrations are ill-defined in parts of the volume V.

For a multiply connected domain, we start by multiplying identity (A2) with the unit normal $\hat{\mathbf{n}}$ from the left, and perform a surface integration over S:

$$\oint_S \hat{\mathbf{n}}\cdot\nabla\wedge(\mathbf{x}\wedge\phi\mathbf{I})\,\mathrm{d}S = -(\mathscr{N}-1)\oint_S \phi\hat{\mathbf{n}}\,\mathrm{d}S - \oint_S [\hat{\mathbf{n}}\cdot(\mathbf{x}\cdot\nabla\phi) - (\hat{\mathbf{n}}\cdot\mathbf{x})\nabla\phi]\,\mathrm{d}S.$$

From Stokes' theorem, the surface integral on the left-hand side vanishes exactly if the scalar ϕ is *single-valued* on the surface S:

$$\oint_S \hat{\mathbf{n}}\cdot\nabla\wedge(\mathbf{x}\wedge\phi\mathbf{I})\,\mathrm{d}S \equiv 0.$$

The last integral on the right-hand side can be rewritten using the elementary vector identity

$$\hat{\mathbf{n}} \cdot (\mathbf{x} \cdot \nabla \phi) - (\hat{\mathbf{n}} \cdot \mathbf{x}) \nabla \phi = \mathbf{x} \wedge (\hat{\mathbf{n}} \wedge \nabla \phi),$$

and equation (B3) is thus recovered. The reader must appreciate that this derivation does not require integrations anywhere else other than on the surface itself. Also, note that this identity requires the scalar ϕ to be single-valued. In this paper, the scalar ϕ just represents the pressure field, which is assumed single-valued from a physical point of view.

An additional useful identity is the time derivative of a surface integral, in which the surface itself is time-dependent (Aris 1962):

$$\frac{\mathrm{d}}{\mathrm{d}t} \oint_{S(t)} \hat{\mathbf{n}} \cdot \Phi \, \mathrm{d}S = \oint_{S(t)} \hat{\mathbf{n}} \cdot \left[\frac{\partial \Phi}{\partial t} + \mathbf{u}_S (\nabla \cdot \Phi) \right] \mathrm{d}S. \tag{B4}$$

Aris (1962) only gives the relation for a vector, but it is easy to generalize it to a tensor.

Finally, for a divergence-free vector $\mathbf{a}$, the following two integral relations may be obtained from identities (A1) and (A3):

$$\int_V \mathbf{x} \wedge (\nabla \wedge \mathbf{a}) \, \mathrm{d}V = \oint_S \hat{\mathbf{n}} \cdot [(\mathbf{x} \cdot \mathbf{a}) \mathbf{I} - \mathbf{x}\mathbf{a} + (\mathcal{N} - 1) \mathbf{a}\mathbf{x}] \, \mathrm{d}S \,, \quad \text{with } \nabla \cdot \mathbf{a} = 0. \tag{B5}$$

$$\int_V \mathbf{a} \, \mathrm{d}V = \oint_S \hat{\mathbf{n}} \cdot (\mathbf{a}\mathbf{x}) \, \mathrm{d}S, \quad \text{with } \nabla \cdot \mathbf{a} = 0. \tag{B6}$$

Equation (B6) is given by Saffman (1993).